Capturing Skin Properties from Dynamic Mechanical Analyses

by

Erika Sandford

S.B. in Mechanical Engineering,
Massachusetts Institute of Technology (2010)

Submitted to the Department of Mechanical Engineering
in partial fulfillment of the requirements for the degree of

Master of Science in Mechanical Engineering

at the

MASSACHUSETTS INSTITUTE OF TECHNOLOGY

June 2012

Author .....
Department of Mechanical Engineering
May 11, 2012

Certified by .....
Lynette A. Jones
Senior Research Scientist in Mechanical Engineering
Thesis Supervisor

Accepted by .....
David E. Hardt
Chairman, Department Committee on Graduate Students

Capturing Skin Properties from Dynamic Mechanical Analyses

by

Erika Sandford

Submitted to the Department of Mechanical Engineering
on May 11, 2012, in partial fulfillment of the
requirements for the degree of
Master of Science in Mechanical Engineering

Abstract

Existing skin mechanical testing devices focus on measuring skin elasticity and are not tailored to assess the dynamic behavior of skin. The mathematical techniques used to analyze data collected using these devices are often not optimal. A new dynamic mechanical device that measures the linear dynamics of skin was developed and tested. The mechanical properties of skin were evaluated in experiments in which the stiffness and damping parameter were measured at different locations on the arm and hand, when stratum corneum hydration was varied by controlled changes in environmental humidity, and following the application of film-forming polymers. Parallel measurements were made with the Cutometer® so that the two devices could be compared.

The findings revealed that reliable and valid measurements of skin mechanical properties can be obtained from the device. The stiffness of the skin was shown to vary significantly as a function of skin site, changes in stratum corneum hydration, and following the application of the polymer films. Changes in the damping parameter were less consistently associated with varying the condition of the skin. The high reliability and speed of measurement make this device and analytic procedure an attractive option for testing skin mechanics.

Thesis Supervisor: Lynette A. Jones
Title: Senior Research Scientist in Mechanical Engineering

Acknowledgments

I would first like to thank my advisor, Dr. Lynette Jones, for being a constant positive source of guidance throughout my time in graduate school. She always provided me with direction for the project while simultaneously encouraging me to develop my own ideas. Dr. Jones taught me a great deal about scientific research and I will be forever grateful for her support.

I would also like to extend my gratitude to Ellen Chen who acted as my mentor while I continued work on the indentometer she originally developed. She generously shared her software and electronics so that I could better understand the project. Ellen is a wonderful teacher and was always there to help whenever I had a question.

I would like to thank Professor Ian Hunter, Dr. Cathy Hogan, and all of the members of the BioInstrumentation Lab for their technical advice and support. Thank you to the lab members, along with many of my other friends, who generously donated their time to act as subjects in my experiments.

I would also like to thank Dr. Greg Hillebrand for providing advice about the test protocols and organizing the purchase and loan of the Cutometer.

I would like to acknowledge one of our undergraduate researchers, Michelle Deng, who compiled information about devices presently used in skin testing studies.

Thank you to Linda Foltis and David Kallal from Ashland Specialty Ingredients for providing the formulations for the third experiment.

Finally, I would like to thank my mom, my dad, my fiance Orrin, and the rest of my family and friends for always believing in me and supporting me throughout my education at MIT.

This work was supported in part by a research contract from Procter and Gamble and by the National Science Foundation.

Contents

List of Figures

List of Tables

Chapter 1

Introduction

The measurement of skin mechanics *in vivo* can provide valuable information about the mechanical properties of skin in both cosmetic and clinical settings. Hydration levels in skin are of particular interest in research in a variety of fields. Cosmetic companies need to test the efficacy of their moisturizing products, while medical professionals need to identify dehydration in patients. The effect of hydration on the skin's mechanical properties is considerable; a high moisture content in the stratum corneum enables a slow rate of transepidermal water loss as well as the appearance of soft, healthy skin. *In vivo* measurements of the skin's hydration level provide a way to characterize the skin's condition, pathological conditions affecting the skin, and the efficacy of moisturizing formulations [1].

Dehydration in a patient is often assessed by touch, in which the skin is pinched, held for a few seconds, and then released (to assess its turgor). Because the information obtained is qualitative, different individuals may vary in their evaluation of the skin's turgor. Cosmetic research relies on a variety of skin testing devices that utilize techniques such as suction and torsion to perturb the skin. Both arenas require a reliable method with which to test hydration, and neither has a standardized process that is fully satisfactory.

Existing skin mechanical testing devices focus specifically on measuring skin elasticity and are not tailored to assess the dynamic behavior of skin. In addition, the

mathematical techniques used in existing approaches are often not optimal. They rely on simple step responses that can theoretically contain a lot of important information which could be described using Burger, Maxwell or Kelvin-Voigt models [2]. The simplification of these important parameters into simple displacement values results in a loss of important dynamic information in favor of expediency. Models, which often do not contain all the necessary dynamics, are then fitted to experimental curves. A more advanced technique that immediately casts the information into relevant parameters such as damping or energy storage/loss is needed.

A device that can characterize the linear dynamic properties of skin and underlying tissue has considerable potential in cosmetology and dermatology where it is essential to describe quantitatively the changes in the mechanical properties of skin associated with a treatment or intervention. None of the existing skin mechanical testing devices can fully characterize the dynamic properties of skin, which is a highly dynamic material. A dynamic mechanical device has been designed and fabricated that can characterize the dynamic behavior of skin in vivo from data acquired in only five seconds. The objective of this research was to evaluate the reliability and validity of the device in characterizing the mechanical properties of human skin on the arm under normal conditions, and to measure the device's performance when the ambient relative humidity was changed and following the application of skin care products.

Motivation for this research and background information about the skin's anatomy is presented in Chapter One. Chapter Two discusses the design of the device developed for the studies conducted in this research. The description includes the mechanical design, as well as the electrical and software designs used. Linear system identification is outlined in Chapter Three. The methods discussed here were used in analyses of the data collected and presented in Chapter Four, which describes the four major experiments conducted. These experiments were conducted on the skin of human subjects *in vivo*. Finally, conclusions from the research are presented in Chapter Five.

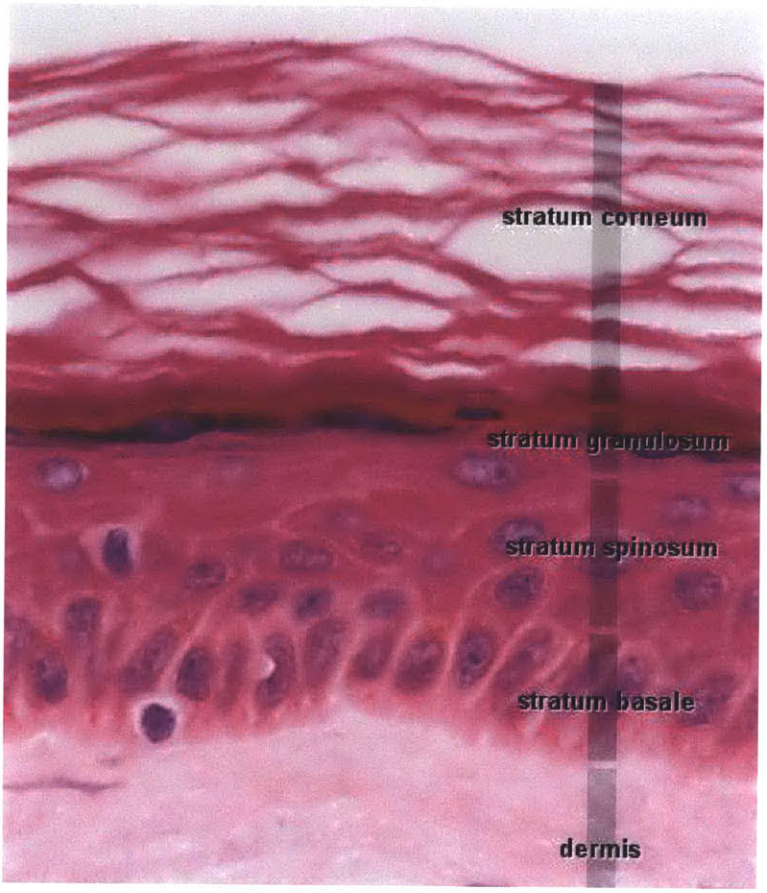

Figure 1.1: The sublayers of the epidermis include the stratum corneum, the stratum granulosum, the stratum spinosum, and the stratum basale [4].

1.1 Characteristics of Skin

The skin is the largest human organ. It is made up many layers, some of which are shown in Figure 1.1. Each layer has distinctive properties and contributes to the overall mechanical properties of the skin. Its purpose ranges from protection from the elements, to temperature regulation, and tactile perception. Glands within the skin produce sweat to prevent the body from overheating. Tiny hairs in hairy skin (see Figure 1.3) help to insulate the skin from cold temperatures. The skin also contains melanin which absorbs ultraviolet light, protecting underlying tissues from harm [3]. Each of these functions is essential to human survival.

Working up from the base of the epidermis, the basal layer is the source for

keratinocytes and cell proliferation. The layer also contains active stem cells. The cells of the basal layer are organized as a series of columns which continue into the next layer, the stratum spinosum. This layer is composed of several layers of densely packed cells, the majority of which are keratinocytes. The only other cells present are lymphocytes and Langerhans cells. This layer is held together by desmosomes. Desmosomes not only provide bonding of the cells, but also contribute to the layer's relatively high tensile strength. Three to four layers of flattened cells comprise the granular layer. This is the region were the keratinocytes begin to die; the nuclei, mitochondria, ribosomes, and other cell components degenerate in this layer [5].

The stratum corneum, the skin's outermost layer, serves as a barrier between the body and the environment. It protects the body as well as other layers of the skin from infection and dehydration. If a virus, fungus, or bacterium penetrates the stratum corneum, it could result in dermatitis or another type of infection. Most of the cells in this 30 cell thick layer are dead; it takes approximately two weeks for skin cells to make the journey to the surface from the basal layer to the stratum corneum, where they are eventually cast off in a process known as desquamation [3].

Originally, the stratum corneum was thought of as a thin plastic film; it was viewed an inert layer that simply covered the skin. Since the 1970s, however, research has concluded that it is a complex and necessary layer that holds water to maintain hydration and acts as a biosensor to signal that the underlying layers should respond to external stresses [6]. In a simple comparison the stratum corneum can be analogized to a brick wall, where keratinocytes serve as the bricks and a lipid extracellular matrix serves as the mortar. This analogy is illutrated in Figure 1.2.

The hydrophobic lipids act as the main barrier to prevent water from permeating into other sublayers of the epidermis. The lipid matrix has a unique composition and organization that has been observed with electron microscopy. It is this organization that blocks water loss from the skin, while simultaneously allowing some moisture absorbancy. The lipid species present include ceramids, fatty acids, and cholesterol [6].

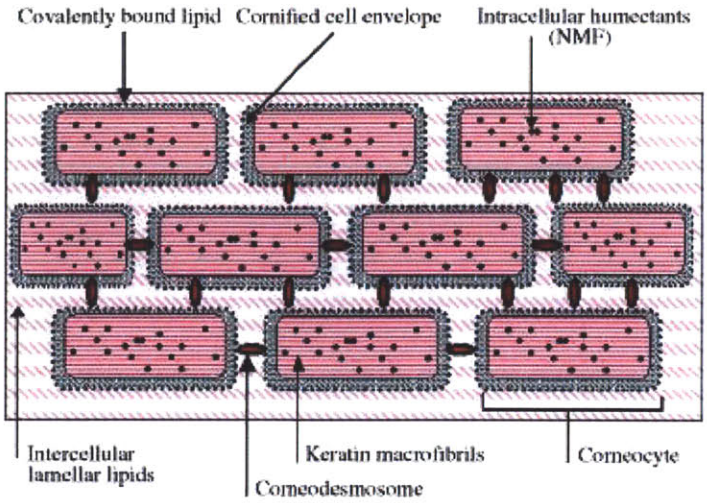

Figure 1.2: Schematic of the bricks and mortar model of the stratum corneum [6].

The mechanical properties of skin primarily depend on the dermal and hypodermal collagen and elastic fiber network that is embedded in a viscous ground matrix, to which the epidermal layer also contributes. The interface of the epidermis and the dermis contains the basal layer's extracellular matrix, basal lamina and anchoring fibrils from the top of the dermis. These fibrils link themselves to bundles of collagen in the matrix, ensuring a connection between the two layers [5].

This research examines the differences in mechanical properties between hairy and glabrous skin, both shown in Figure 1.3. Glabrous skin, found on the palms, the soles of the feet, and the lips, has a thick epidermis, with a stratum corneum thickness that ranges from 100 to 200 μm. Conversely, the stratum corneum of hairy skin ranges from 10 to 40 μm. Glabrous skin is anchored to the underlying fascial planes by fibrous tracts which prevent the skin from gliding over the underlying tissue. These structural differences between the two types of skin are expected to contribute to differences in the overall skin dynamics.

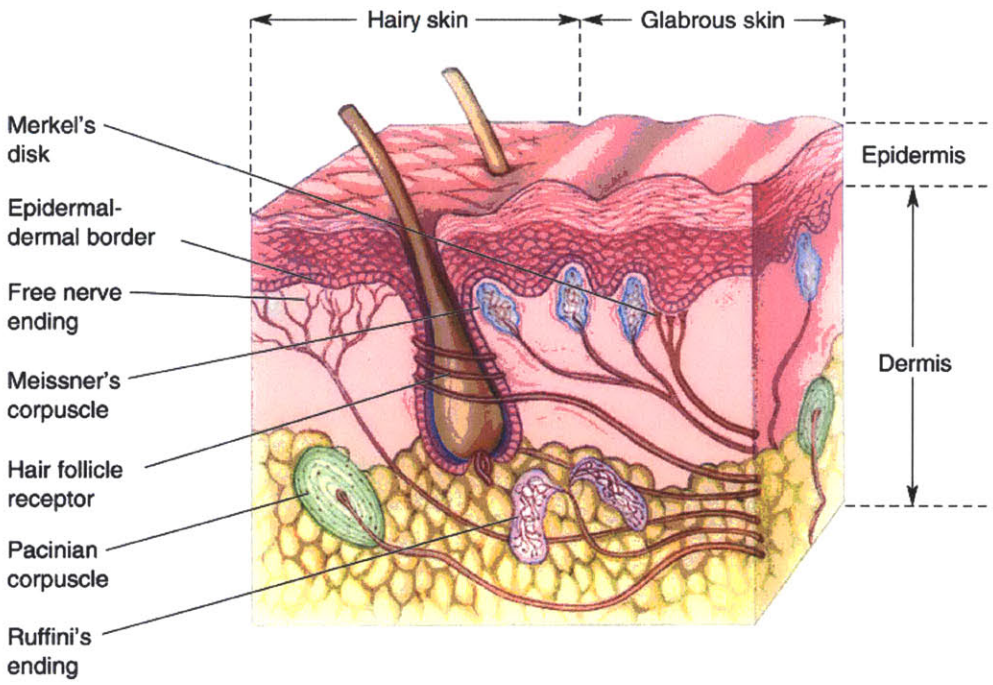

Figure 1.3: Hairy skin, shown on the left, contains hair follicles, while glabrous skin does not [7]. Glabrous skin can be found on the soles of the feet, the palm of the hand, and the lips.

1.2 Devices for Tissue Characterization

A variety of instruments are used to measure the mechanical properties of human skin *in vivo* including skin rheometers, cutometers and indentometers all of which provide information about the mechanical properties of skin [8], [9]. These devices use a range of techniques to measure skin mechanics *in vivo*, including suction, indentation, torsion, extension, ballistometry, and wave propagation. Typically stress-strain relations and measurements of creep and stress relaxation times are measured as a probe indents the skin at a fixed velocity or force or as the skin is lifted, stretched and released [10], [11]. As the pressure or torque of the device increases, the skin first displaces elastically and then creeps once it enters the viscoelastic region. When the system becomes stationary, the device is usually timed to release the pressure or torque, after which the skin relaxes. The application of pressure or torque will normally cause the tissue to have some long-term deformation which means that the skin does not return to its original state for some time.

Devices such as the Cutometer® (Courage and Khazaka) and the Dermalab (Cortex Technology) use a suction mechanism in which a pump applies a constant negative pressure at the probe head. The skin in contact with the probe is pulled up into the probe and sensors mounted in the head of the probe measure the maximum displacement of the skin. This process is inherently nonlinear in that a linear increase in pressure does not result in a proportional increase in the displacement of the skin. Different displacement parameters that represent the elastic, viscoelastic, relaxation, and total displacement properties of the skin are typically calculated from the data sampled and compared across different sites. Each measurement can take up to 60 seconds before the skin has reached a stationary state for the pressure or torque applied, which can make the tests conducted by these instruments long if many measurements are taken. The results have also been shown to vary as the number of cycles increases due to progressive creep [12].

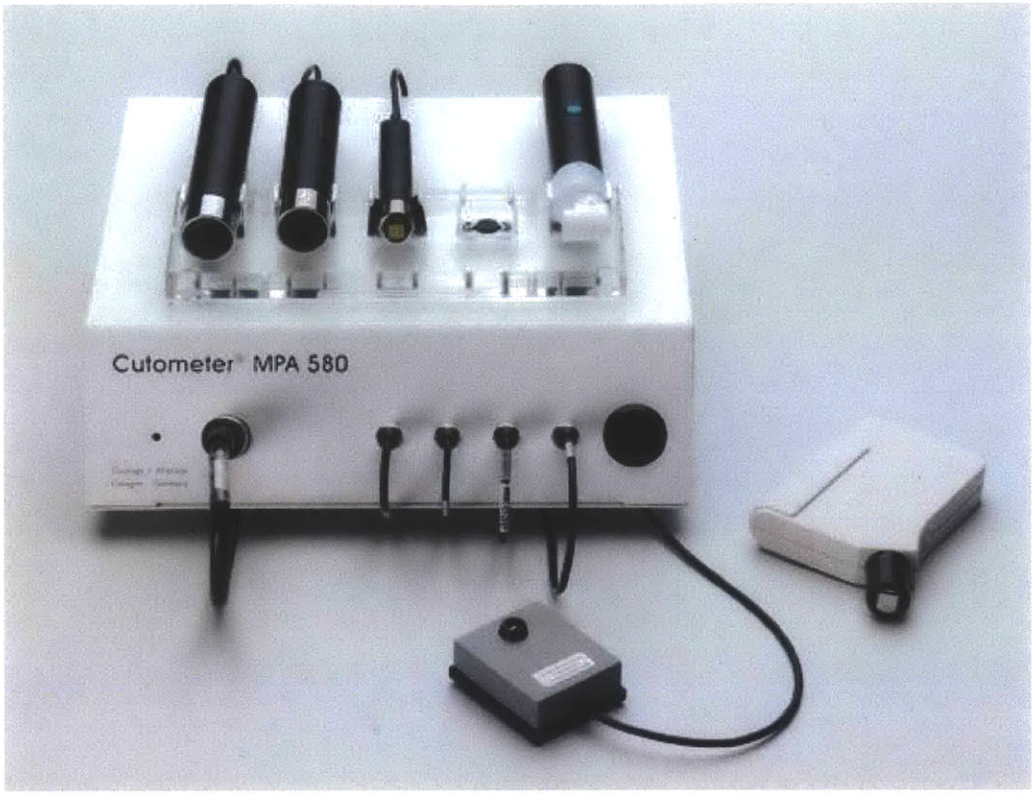

Figure 1.4: The Cutometer MPA 580 by Courage and Khazaka. [15]

1.2.1 Cutometer

The Cutometer is commercially available and used by cosmetic companies and other researchers to assess the mechanical properties of the skin. It is often regarded as the "gold standard" against which other skin mechanical testing devices are compared [13]. Courage and Khazaka has developed several Cutometer models, including the SEM 474, the SEM 575, the MPA 580, and the Dual 580. The SEM 474 is the oldest version of the device; it works with DOS software and is not compatible with modern PCs. The SEM 575 was the next iteration of the device and it works with Windows software. However, it only works with one probe and has a low sampling rate. The MPA 580 has a higher sampling rate and can connect to four different sized probes. The Dual 580 is the newest Cutometer model and will be released for sale May 1st, 2012. It can connect to six different probes [14]. The device used in this research was the Cutometer MPA 580, shown in Figure 1.4.

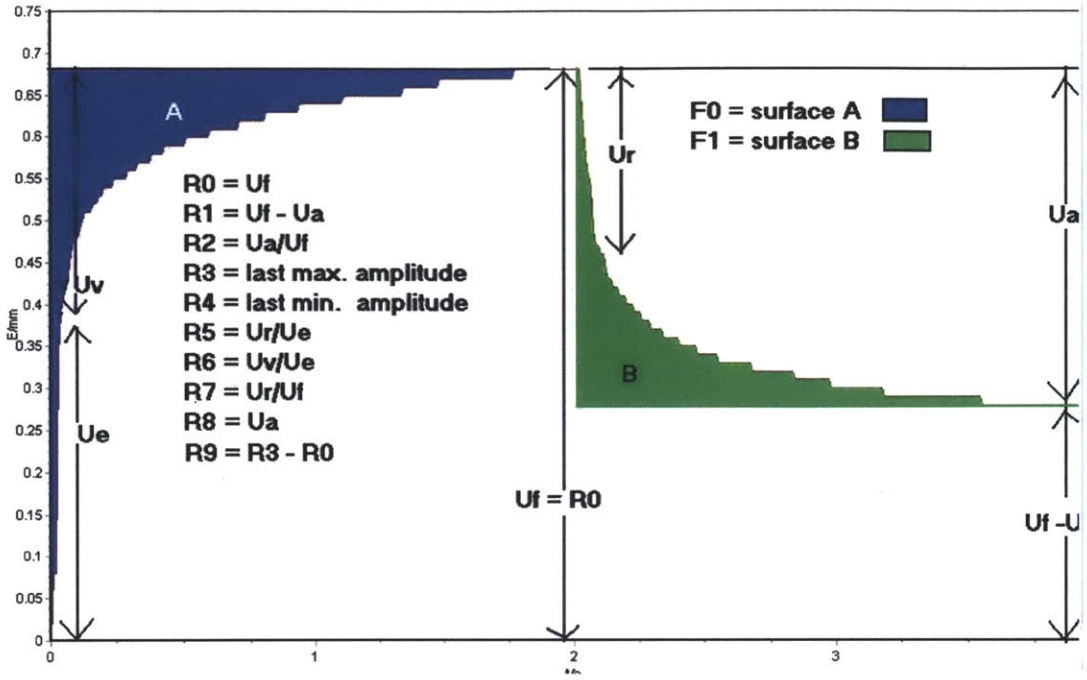

Figure 1.5: Output parameters of the Cutometer MPA 580 [16].

The device uses suction to pull the skin into the aperture of the probe. An optical system inside the probe measures the penetration depth of the skin. The instrument has a sampling rate of 100 Hz. The measuring probe used for this research had a 2 mm aperture diameter. Other probes are available with aperture diameters of 4 mm, 6 mm, and 8 mm. The 2 mm probe allows measurement of skin layers closer to the surface, while the larger diameter probes are able to deform deeper layers of the skin, such as the dermis. Deformation of the skin increases linearly as a function of the probe's diameter [1].

The resistance of the skin to suction and its ability to return to its original position are given at the end of each measurement. The output parameters include elastic deformation, retraction, viscoelasticity, and ratios involving each of these, as shown in Figure 1.5. In this research the following parameters were calculated: R0 (U_f, the elastic deformation of the skin), R5 (U_r/U_e, the pure elasticity without viscous deformation), and R6 (U_v/U_e, ratio of viscoelastic to elastic extension).

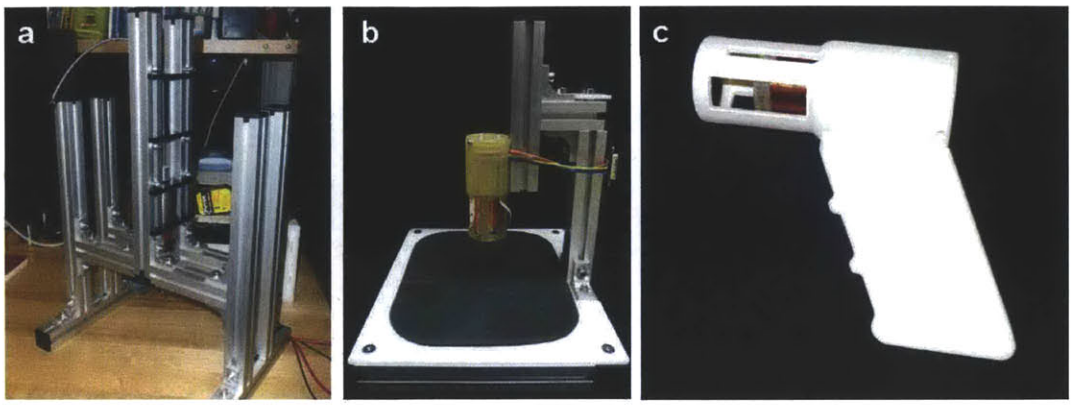

Figure 1.6: (a) The prototype, (b) desktop version, and (c) hand-held version of Chen's indentometer for nonlinear system identification. [17]

1.2.2 Indentometer

Chen developed an indentometer, shown in Figure 1.6, capable of conducting linear and nonlinear system identification on skin and other biological tissues *in vivo*. During operation, the device is oriented perpendicular to the skin and its probe perturbs the tissue with an up and down motion. As shown in the figure, the indentometer can be configured as a desktop device (b) or a hand-held version (c). The hand-held version is practical for clinical applications because it is lightweight and relatively inexpensive to manufacture [17], [18].

This device is intended for nonlinear system identification of biological tissues. The indentometer and the techniques developed by Chen can be used for characterizing the biomechanical properties of tissue.

1.2.3 Other Devices

The Corneometer CM 825 (Courage and Khazaka, Köln, Germany), shown in Figure 1.7, measures the capacitance of the stratum corneum. Changes in hydration produce corresponding changes in the capacitance measurements. The device operates at a mean frequency of 1 MHz. It includes a probe that contains ceramic tile with many gold electrodes that act as capacitor plates. The probe's area is 49

Figure 1.7: Corneometer CM 825 [16].

mm^2. The measurements are provided in arbitrary units that range from 0 (very dry) to 120 (very wet) a.u. [16].

The Dermal Phase Meter 9003 (NOVA Technology Corporation, Manchester, MA, USA) measures the skin's electrical impedance. The device has a variety of probes available for making measurements. It takes measurements at different frequencies of the applied current.

The Reviscometer (Courage and Khazaka, Köln, Germany) is a device that measures the propagation of shock waves along the skin. It emits a wave in the direction of the skin's fibers and has a receiver that picks up the wave a certain distance away from the source. The device is used to determine the condition of the collagen and elastin fibers in the skin, and is often used in ageing studies.

Dia-stron's Dermal Torque Meter, pictured in Figure 1.9 uses a central disk that is attached to the skin with an adhesive tape. A concentric outer ring remains stationary while a torque is applied to the inner disk. The degree of rotation is measured. The size of the gap between the central disk and the outer ring is critical because it determines the depth of penetration into the skin, and what layer of skin will be measured. The Dermal Torque Meter is used for measurements of

Figure 1.8: Reviscometer RVM 600 [19].

stratum corneum elasticity, hydration, and friction in the skin. Changing the gap size could also allow measurement of hydration in other skin layers [20]. According to some researchers, the device is more sensitive than the Cutometer for hydration testing [13].

Courage and Khazaka's Frictiometer FR 700 applies a constant rotational speed to the skin by the friction head. Different heads are available for applying different friction levels between the probe and the skin. The device measures the torque and displays results in Frictiometer units. The Frictiometer has been used to distinguish between normal and dry skin. It can also be used for before and after comparisons with gels, peels, and other skin care treatments [21].

The Venustron by Axiom, displayed in Figure 1.10, measures skin elasticity and relative firmness. It has also been used in studies investigating the effects of athletic training on muscle fatigue and the skin. The device acquires data in a manner similar to the indentometer; the probe is placed above the skin and a motor inside the probe is activated to push the sensor tip down to the skin. After the probe touches the skin it retracts. The Venustron has a sampling frequency of 200 Hz. The software outputs hysteresis curves based on the probe's interaction with the skin [22].

Cortex Technologies manufactures the DermaLab, which can be used to measure

Figure 1.9: Dermal Torque Meter [20].

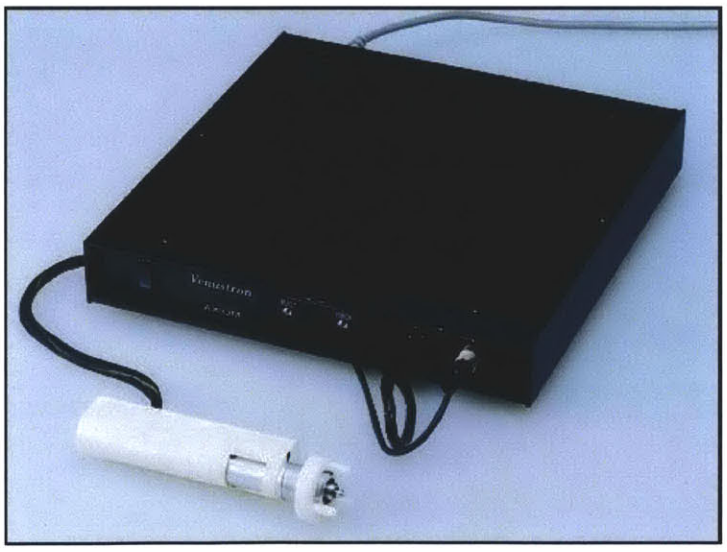

Figure 1.10: The Venustron by Axiom [22].

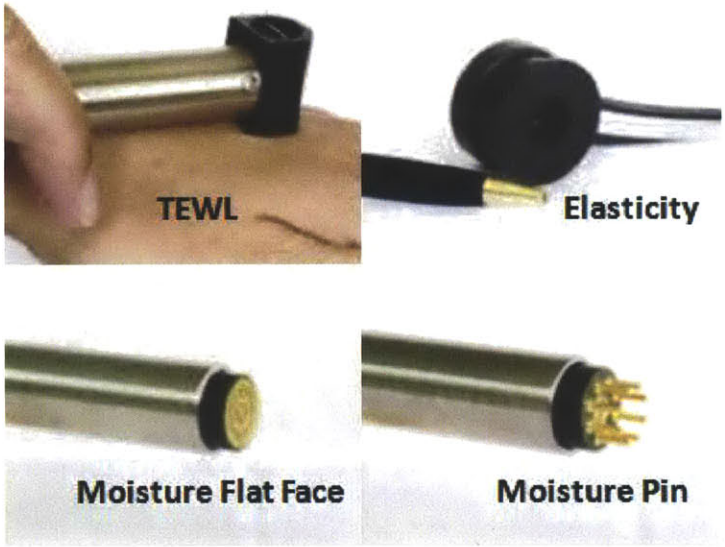

Figure 1.11: The DermaLab by Cortex contains probes for measuring transepidermal water loss, elasticity, and moisture [23].

the skin's Young's modulus, viscoelasticity, and hydration. The device's different probes are pictured in Figure 1.11. The DermaLab interfaces with LabVIEW based software. The system contains several modules for the different measurements it performs. To measure transepidermal water loss, it relies on the vapor gradient principle. It measures conductance in the stratum corneum for hydration readings. The elasticy module operates like the Cutometer by applying suction to the skin [23].

Finally, the Torsional Ballistometer (Dia-stron) is a hand held instrument that can be used to determine the skin's dynamic resilience and firmness. The device is shown in Figure 1.12; it contains a long, slim probe with a rigid arm suspended by a wire. The arm is activated by a solenoid, which elevates the probe tip above the test sample. The probe tip bounces on the surface, and its position is measured. The position changes based on the sample's mechanical properties [20].

Figure 1.12: The Torsional Ballistometer by Dia-stron [20].

1.3 Summary of Research

The aim of this research was to measure the reliability and validity of the device developed by Chen and to determine how the mechanical properties of skin changed as a function of hydration and the application of film-forming polymers. The device was named the Dynamic Mechanical Device (DMD) and it was configured so that it applied both normal and tangential forces to the skin. The motivation for developing the DMD was to have an instrument that provides quick, reliable measurements of the skin's mechanical properties. This research focused on measuring the properties of the stratum corneum. The linear mechanical properties measured were stiffness, the damping parameter, and natural frequency.

A series of experiments was conducted to characterize the device's reliability and validity, and to assess its performance as the state of the skin changed. First, the DMD was characterized so that its properties could be separated from the measured properties of the skin. The first set of experiments involved testing the skin with

both the DMD and the Cutometer MPA 580, for the purpose of comparing the DMD's reliability to that of the industry standard. The DMD's validity was then established in a series of experiments where it was used to test artificial skin samples with known mechanical properties. Next, the mechanical properties of the skin on five different body sites were measured in males and females. These sites included both hairy and glabrous skin. Following these studies, measurements were made on untreated female skin and these were compared with measurements of the skin made after it had been treated with various formulations. These formulations contained film-forming polymers, such as Aquaflex and Styleze. Finally, the effects of varying the hydration of the skin on its mechanical properties were measured.

Chapter 2

Dynamic Mechanical Device

2.1 Mechanical Design

A dynamic mechanical device was designed and fabricated for this research. The device is capable of identifying the linear dynamic properties of human skin *in vivo*. The design of the DMD was based on Chen's indentometer, and was constructed as a high bandwidth, high displacement instrument for surface mechanics testing [17], [18].

The DMD comprises a custom built Lorentz force actuator that has an inner diameter of 25 mm. The actuator contains a coil that was custom wound around a bobbin printed by stereolithography. The coil, which was wound with six layers of 28 gage wire, has a resistance of 14 Ω. It is designed as an overhung configuration; that is, the coil windings extend beyond the height of the magnetic field gap. The actuator and probe are housed in a custom fit case that was fabricated using stereolithography. The case is affixed to a bench top aluminum frame. The solid model of the device and the device itself are pictured in Figures 2.1 and 2.2, respectively.

A Lorentz force coil was chosen for the design because it allows direct force control, which means a real-time controller is not needed and internal feedback in eliminated. It has a high bandwidth, is capable of high forces, and has a long stroke. It is also a relatively low cost option because of its straightforward design [17], [18].

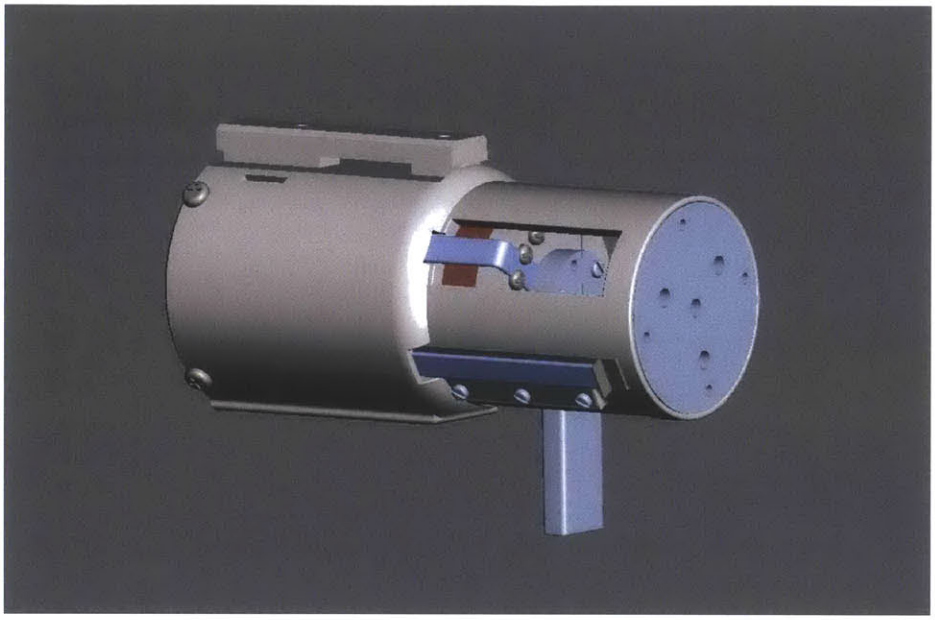

Figure 2.1: SolidWorks assembly model of dynamic mechanical device.

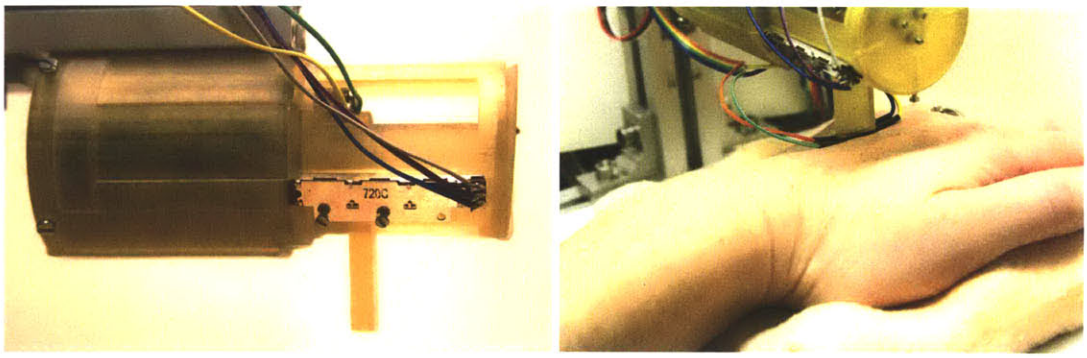

Figure 2.2: Indentometer device modified for surface mechanics testing.

The Lorentz force, which is the force on a point charge in an electromagnetic field, provided by the coil is given by

$$F = ILN \times B, \tag{2.1}$$

where F is the Lorentz force, I is the current perpendicular to the field, and N is the number of conductors in series with length, L. B is the magnetic field strength [17].

The actuator has a stroke of approximately 30 mm, which is limited by a spring that connects the edge of the probe to the end of the device, as shown in Figure 2.3. The spring acts to pull the probe back over the skin during the measurement period. The rectangular tip of the probe has a 5 mm by 12 mm contact area. Other probes can be attached to the device for different measurement purposes.

An ALPS linear potentiometer (model RDC10320RB) is attached to the coil to measure the position of the actuator. A Honeywell miniature force sensor (model FSS1500NS) is attached to the tip of the probe that makes contact with the skin to ensure that the normal force between the probe and the skin remains within the specified range (1.2-1.5 N) at the beginning of the experiment. The force sensor contacts the skin with a spherical tip that has a 1.5 mm diameter.

A custom electric circuit designed for the indentometer by Chen was used in the DMD's electronic design. A voltage is provided to an amplifier which sends a current to the linear actuator. The actuator contributes a force to the attached probe, which is contacting the skin. The position and force of the probe are measured as it moves over the skin. Stochastic system identification techniques developed by Hunter and Korenberg are used to characterize the system, which includes both the device and the skin [24], [25], [26], [18]. Contact between the probe and skin is maintained throughout the process. A schematic of this system is shown in Figure 2.4.

Two Burr-Brown OPA 594 linear amplifiers make up the amplifier for the system. Position and force are sampled by 16-bit resolution analog-to-digital converters (ADCs). The coil is driven by a 48 V power supply, which is powered by a Mean Well AS120P48P1M AC power adapter. The sensors are powered with an Agilent

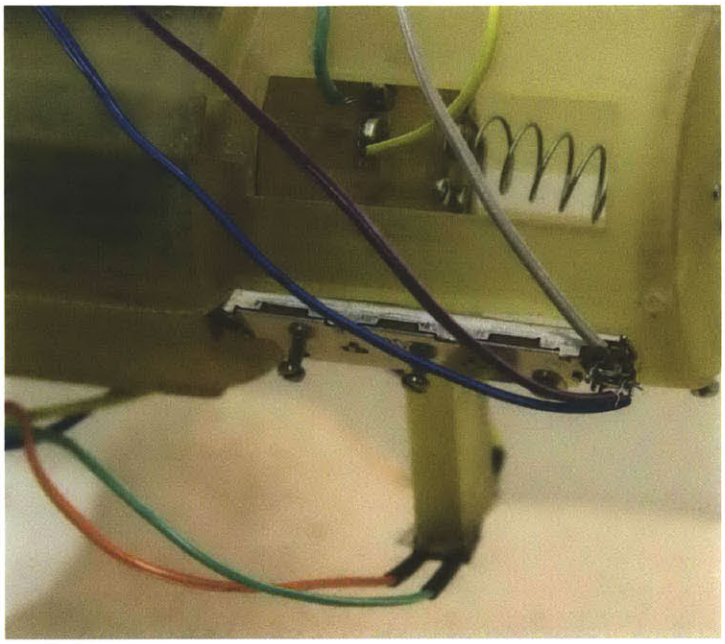

Figure 2.3: Close-up showing spring that connects the edge of the probe to the end of the device.

E3631A power supply. With two separate power sources, power supply noise is reduced and the signal quality provided to all parts of the device is increased. Data acquisition is carried out with a National Instruments USB-6215.

2.2 Software

The software used in this research was originally developed by Chen for the indentometer [17]. This section will serve as a summary of this software and how it was modified and used for the DMD. Calibration and data acquisition were performed in LabVIEW 10.0 (National Instruments), which also displayed the data and was used to perform preliminary system identification. More complex system identification was conducted in MATLAB.

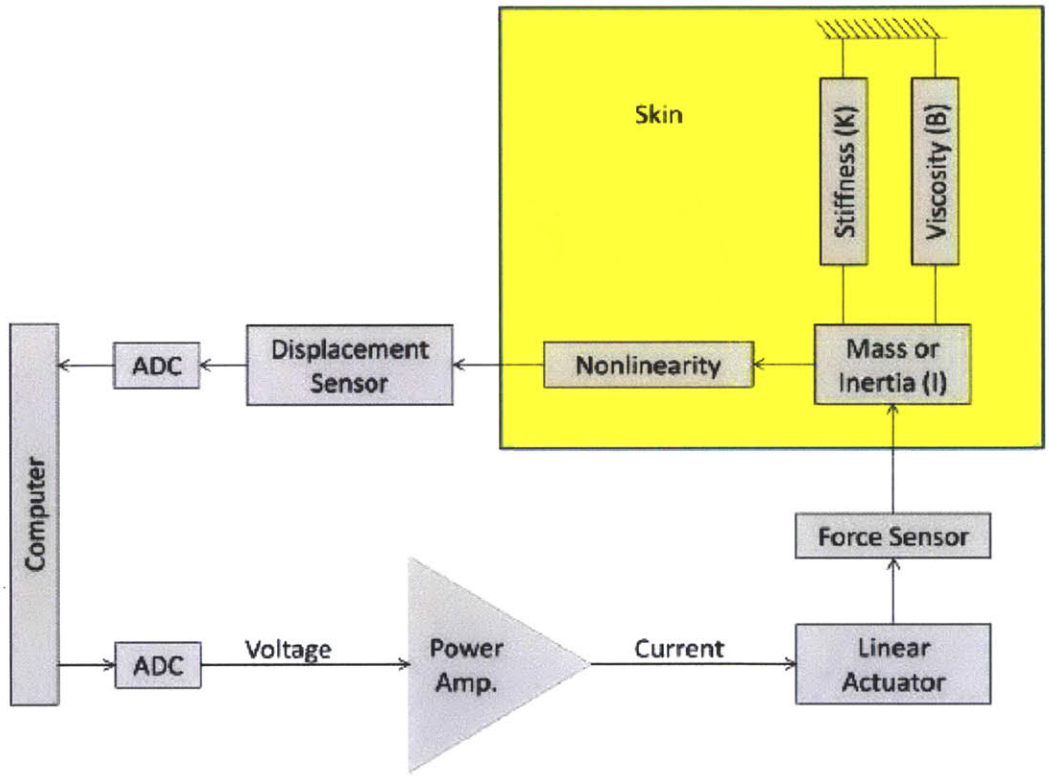

Figure 2.4: A schematic of the experimental system.

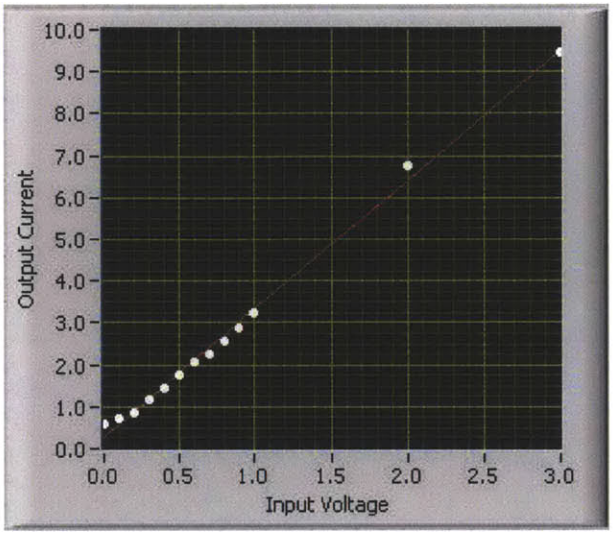

Figure 2.5: The static calibration curve illustrating an input voltage and the measured current in the coil.

2.2.1 Calibration

The software includes static and dynamic calibration systems to assess the performance of the DMD. Initially, the system being measured includes the device as well as the skin. Calibration is necessary to identify the properties associated with the device so that they can be removed from the system to reveal the skin's properties.

The static calibration consists of two steps. The first step involves a manual force to current calibration. In the second step, a voltage is applied to the coil at different constant values and measures the current, which results in a linear curve, shown in Figure 2.5. The sensors on the device are also calibrated in this way. This calibration essentially compares the static input voltage to the static force, which is shown together with position in Figure 2.6. After the process is completed, the constants are saved to be read during system identification [17]. The GUI used for static calibration is shown in Figure 2.7.

Next the system undergoes dynamic calibration, during which the performance of the coil is analyzed at different positions along its horizontal track. The position of the coil is varied and data is sampled at 2 kHz. The software performs system

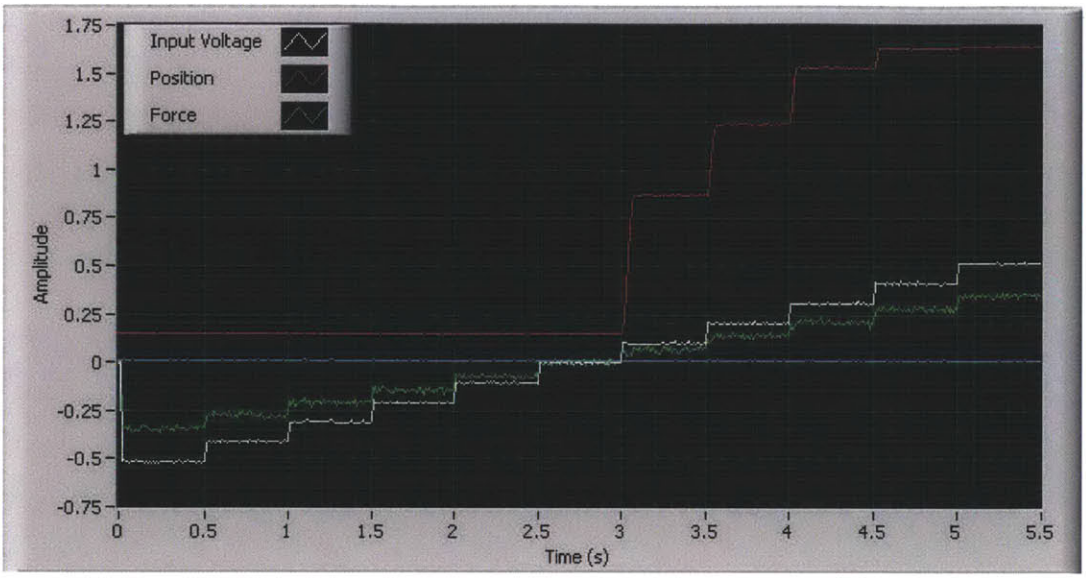

Figure 2.6: The static calibration interface showing input voltage in white, force in green, and position in red.

identification on the coil to identify the linear region in all of its possible positions. Ideally, the Lorentz force will remain linear during the coil's entire movement. Dynamic calibration uses the same stochastic input that is discussed in the General Experimental Protocol (Chapter Three) for skin testing. This calibration can be viewed as testing the properties of the device only; in contrast, the experiments tested properties of the device and the skin combined. Because all measurements are linear, the coil's known properties derived from the calibration can be removed from the final experimental data, leaving only the skin's properties.

The Lorentz force in the entire region traveled by the coil does remain linear because the spring connecting the probe and bobbin to the end of the device acts to keep some part of the coil within the magenetic field at all times. The Lorentz force becomes nonlinear in the indentometer at the coil's farthest position because most of the coil has left the magnetic field [17]. Because the coil never completely leaves the field in the DMD's configuration, nonlinearities are not introduced into the Lorentz force and can be neglected.

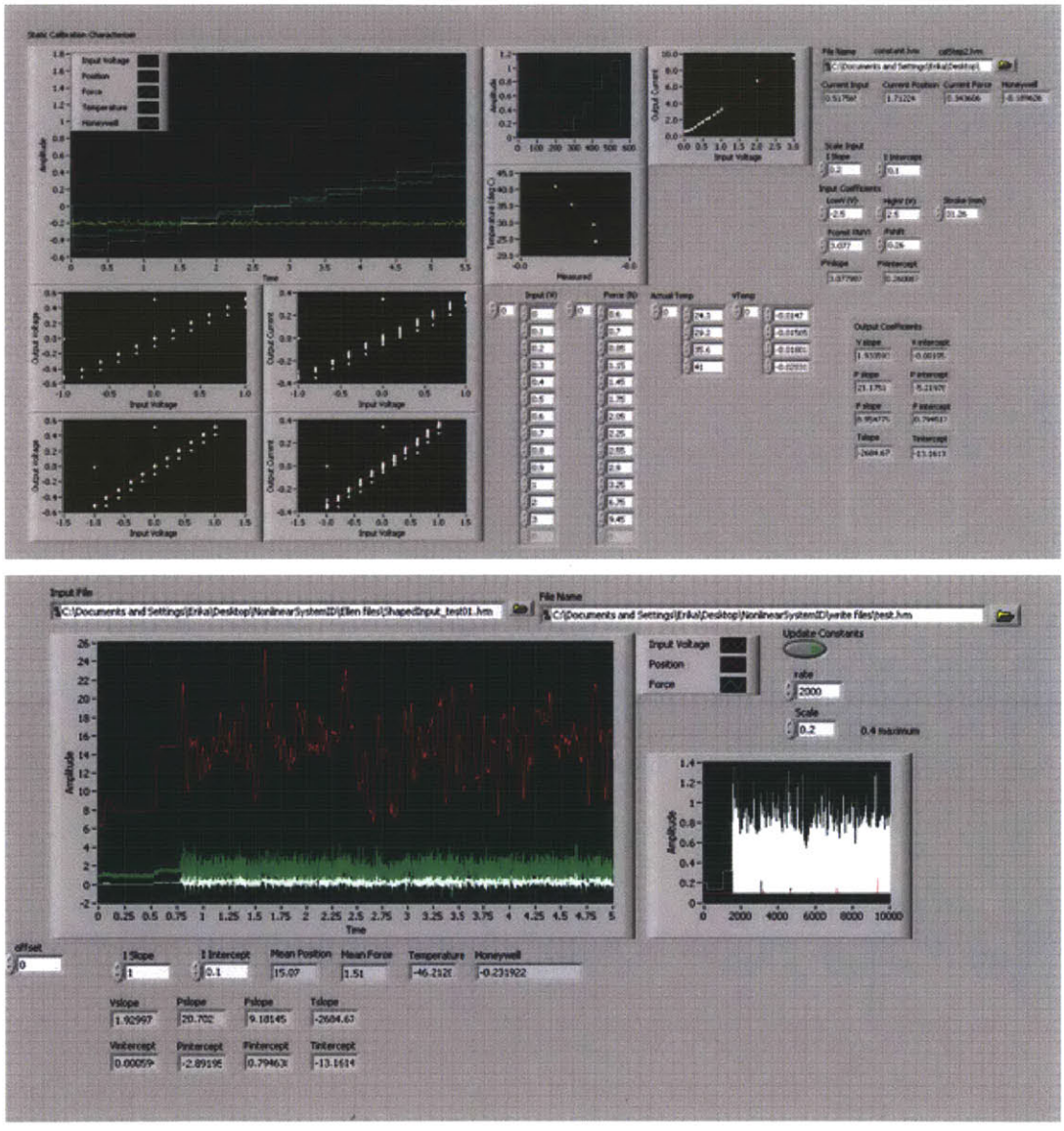

Figure 2.7: Static (top) and dynamic (bottom) calibration software in LabVIEW 10.0.

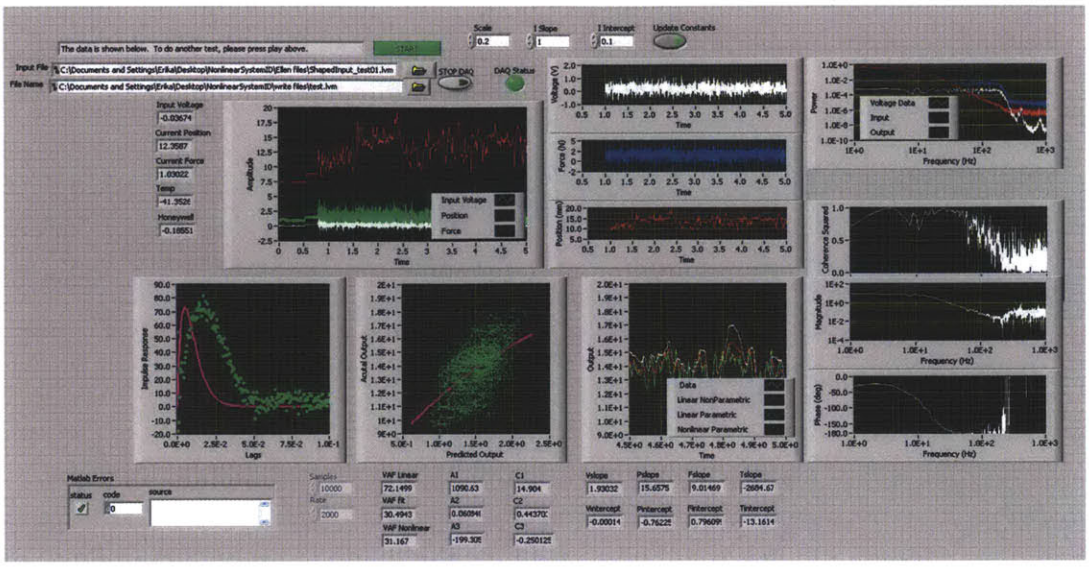

Figure 2.8: System identification software in LabVIEW 10.0. The software takes measurements, performs system identification, and displays preliminary data.

2.2.2 System Identification

The LabVIEW system identification software, shown in Figure 2.8, takes measurements, performs system identification, and displays data. After measurements and preliminary analyses are done in LabVIEW, the data are analyzed in MATLAB using more advanced system identification techniques.

The software applies a stochastic input to the DMD. The outputs include the damping parameter, natural frequency, spring constant, mass, damping coeffecient, and variance accounted for. These outputs are discussed in more detail in Chapter Four.

Impulse responses, which show the system's output when presented with a brief input pulse, were recorded for every measurement. These fully characterize the dynamics of the linear system and show the change that occurs in the spring constant and damping parameter under different conditions. Linear system identification will also be discussed in more detail in Chapter Four.

Chapter 3

General Experimental Protocol

The experiments presented in Chapter Five were conducted with the DMD. The Cutometer MPA 580 was also used in Experiments 1, 2, and 4. The room temperature where testing was conducted was maintained at approximately 20°C. The ambient relative humidity was approximately 45%. Subjects were seated with their arm fixed at a 90° angle at the elbow for both DMD and Cutometer testing. The following outlines the general protocol followed for each experiment.

3.0.3 Dynamic Mechanical Device

The skin on the site being tested was initially placed under the force sensor on the probe's tip. The normal force exerted by the probe on the skin was maintained between 1.2 and 1.5 N, which resulted in the skin being indented by 1-2 mm. This range of forces was selected based on pilot experiments which showed that the most consistent measurements of stiffness and damping, as defined by a coefficient of variation of 5% or less, were obtained when the normal force was maintained within this range. Calibrations were performed at the beginning of each set of measurements to measure the contact force of the probe on the skin. If necessary, the height of the device was adjusted so that the normal force was within the specified range. If a subject moved his or her hand or arm during the experiment, the force calibration procedure was repeated.

The tangential forces delivered to the skin by the device consisted of a Gaussian stochastic input with a tailored power spectrum having a cutoff frequency of 200 Hz. This cutoff frequency was chosen because it is well above the natural frequency of the skin under study. The stochastic force input was low-pass filtered to boost lower frequencies where it would be expected that the skin mechanics have a higher force to displacement (compliance) gain. The resulting band-limited stochastic signal is a powerful probe for identifying linear dynamic systems. Each trial lasted 5 seconds and eight consecutive measurements were taken at each location. The data were sampled at 2 kHz.

3.0.4 Cutometer

For experiments in which the Cutometer was used, four measurements were taken at the designated sites. The time/strain mode was used in all experiments. Each measurement lasted 10 seconds. In the initial 5 seconds a constant negative pressure of 400 mbar was applied to the skin, followed by a 5 second relaxation period. The data were sampled at 100 Hz with the 2 mm aperture probe.

3.0.5 Coefficient of Variation

The DMD and the Cutometer provide results in different units of measurement, so their results cannot be compared directly. However, the reliability of the two devices can be compared by examining their coefficients of variation. The coefficient is a commonly used index of the consistency of a device's performance [27], [28]. It is defined as

$$CV = 100 \cdot \frac{SD}{\bar{x}}, \tag{3.1}$$

where SD is the standard deviation of the sample and $\bar{x}$ is the mean. Multiplying by 100 allows the coefficient of variation to be expressed as a percentage. A reliable measuring instrument would be one with a coefficient of variation of 5% or lower.

3.0.6 Subjects

Male and female subjects participated in the skin studies. All subjects were healthy and did not have any neurological or dermatological conditions that would have affected the skin. Each subject gave informed consent, and all research was approved by MIT's Institutional Review Board.

Chapter 4

Linear System Identification

Non-parametric compliance impulse response functions, which are a complete description of the linear dynamic relation between the force input and the displacement output, were calculated for each trial using a least mean squares method involving Toeplitz matrix inversion. This involves deconvolving the input auto-correlation function from the input-output cross-correlation function. The overall system dynamics included both the skin and actuator dynamics, but after the device was calibrated, its effects could be removed from the data.

The non-parametric impulse response functions were well approximated by second-order under-damped low-pass parametric impulse response functions. The general form of the fitted second-order low-pass under-damped impulse response can be obtained from the inverse Laplace transform of the system's compliance transfer function:

$$H(s) = \frac{1}{Is^2 + Bs + K}, \tag{4.1}$$

or equivalently,

$$H(s) = \frac{Gain \cdot \omega_n^2}{s^2 + 2\zeta\omega_n s + \omega_n^2} \tag{4.2}$$

where K is the stiffness, B is the viscous damping, and I is the inertial term. ω_n is the natural frequency of the system, $Gain$ is the static compliance, and ζ is

the damping parameter. Note that

$$Gain = \frac{1}{K}, \tag{4.3}$$

$$\omega_n = \sqrt{\frac{K}{I}}, \tag{4.4}$$

and

$$\zeta = \frac{B}{2\sqrt{I \cdot K}} \tag{4.5}$$

or equivalently,

$$I = \frac{1}{Gain \cdot \omega_n^2}, \tag{4.6}$$

$$B = \frac{2\zeta}{Gain \cdot \omega_n}, \tag{4.7}$$

and

$$K = \frac{1}{Gain}. \tag{4.8}$$

The inverse Laplace transform of the compliance transfer function, $H(s)$, is the compliance impulse response function, $h(\tau)$. For the case where the system is underdamped (ζ<1),

$$h(\tau) = Gain \cdot \omega_n \cdot e^{-\zeta\omega_n t \cdot \frac{sin(\sqrt{1-\zeta^2} \cdot \omega_n t)}{\sqrt{1-\zeta^2}}}. \tag{4.9}$$

The impulse responses for each trial were calculated using a least mean squares method with Toeplitz matrix averaging. This method compares the stochastic input with the output and attempts to locate the correlated components. The impulse response for skin was determined to be second order, shown in Figure 4.1.

The general form of the fitted second order impulse response can be obtained

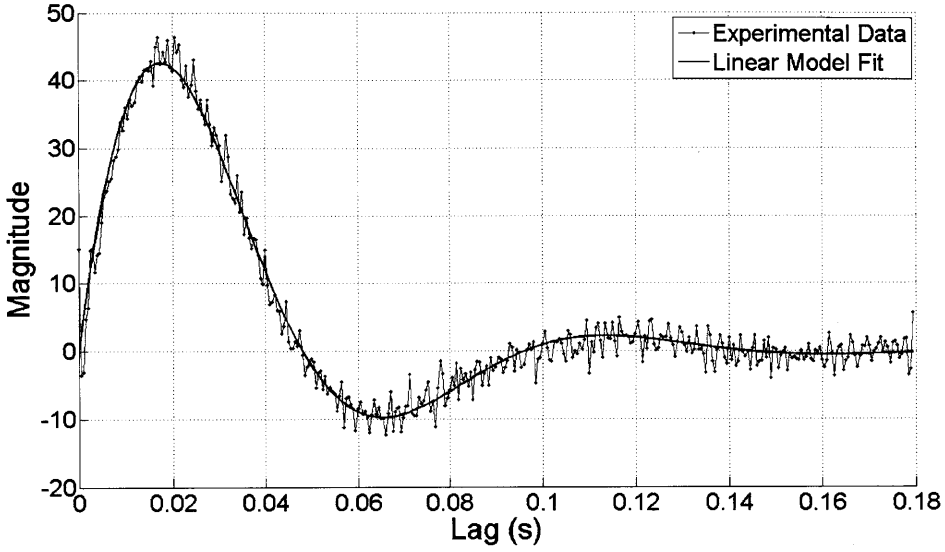

Figure 4.1: Second order impulse response with linear model fit.

from the inverse Laplace transform of the system's output,

$$h(t) = A_1 sin(A_2 t) e^{A_3 t}, \tag{4.10}$$

where h(t) is the impulse response, A_1, A_2, and A_3 are the fitted parameters, and t is the lag in seconds.

A good deal of information about the system can be determined from simply looking at the impulse response. For example, the system illustrated in Figure 4.1 is underdamped because the impulse response starts out positive and becomes negative before beginning to settle; this means the damping parameter is less than one. The quick settling time of the response, however, indicates that the damping parameter is relatively high.

To measure the quality of the fit, the Variance Accounted For (VAF) by the model can be calculated. The VAF is expressed as a percentage and expresses how well the model fits the measured data. VAF is defined as

$$VAF = 1 - \frac{\sigma_{y-y^*}}{\sigma_{y^2}}, \tag{4.11}$$

where σ_{y-y^*} is the standard deviation between the measured and predicted outputs and σ_{y^2} is the standard deviation of the measured signal [17].

Chapter 5

Skin Studies

5.1 Experiment 1: Artificial Skin Samples

5.1.1 Objective

The purpose of this study was to test the reliability of the DMD on artificial skin samples before testing human subjects, and to provide baseline data from which the DMD could be evaluated. The artificial skin samples had been used in previous studies [12] and were designed to exhibit mechanical properties similar to human skin. It was hypothesized that if the device could detect differences among the artificial samples, it had a greater potential of measuring dynamic skin properties *in vivo*.

5.1.2 Procedure

An initial series of experiments was conducted using the DMD and the Cutometer MPA 580 to compare the mechanical properties of six artificial skin samples. The samples (Beaulax, Tokyo, Japan) were each a 50 mm square that was 5 mm thick. The skin samples, shown in Figure 5.1, had a range of mechanical properties and were denoted as 0.20 (softest), 0.21, 0.22, 0.23, 0.24, and 0.25 (hardest). These numbers are arbitrary units. These are the same artificial skin models used in the

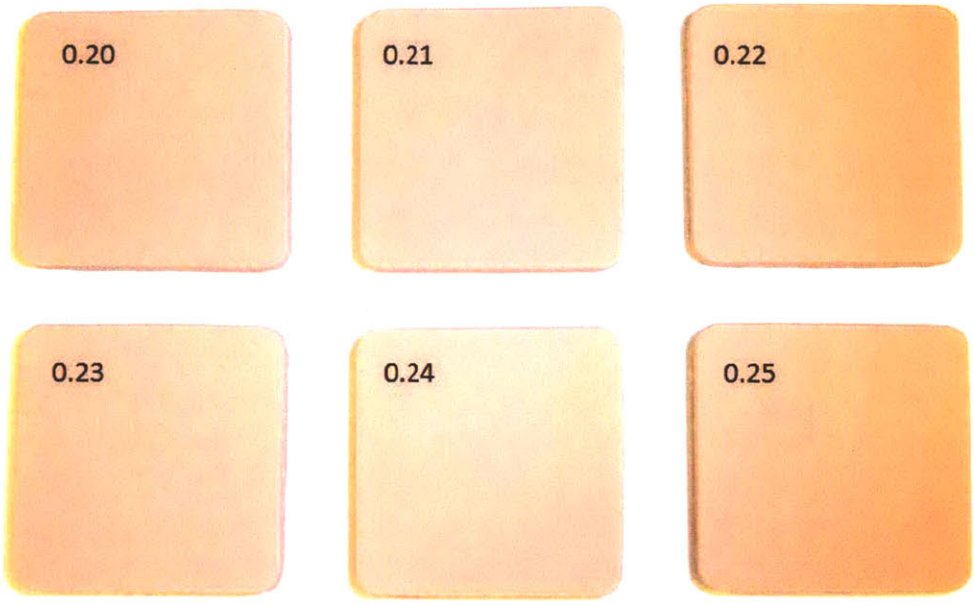

Figure 5.1: The six artificial skin samples tested, with softnesses ranging from 0.20 to 0.25.

indentometric analysis of skin by Jachowicz et al. [12]. The samples were affixed to the flat surface beneath the DMD's probe with double sided tape to ensure no slipping would occur.

The procedure described in Chapter Three was used. Each trial lasted five seconds and eight consecutive measurements were taken of each sample.

5.1.3 Results

5.1.3.1 DMD

Nonparametric compliance impulse response functions calculated from the data from the artificial skin samples with the two most extreme mechanical properties (0.20 and 0.25) are shown in Figure 5.2. It can be observed that the 0.20 sample has a damping parameter close to 1 because its impulse response only barely becomes negative. The 0.25 sample has a damping parameter much lower than 1, which is reflected in the oscillation seen in the figure. The 0.20 sample also exhibits a lower

Table 5.1: Coefficients of variation (CV) for artificial skin sample testing with the DMD.

Artificial Skin Sample Number	Damping Parameter CV	Stiffness CV
0.20	4.8%	4.3%
0.21	3.8%	4.6%
0.22	2.4%	2.1%
0.23	3.3%	3.6%
0.24	4.8%	4.6%
0.25	2.6%	2.4%
Average CV	**3.6%**	**3.6%**

peak value than the 0.25 sample, which translates to a lower spring constant.

The impulse response functions were fitted with Equation 4.10, the inverse Laplace transform of the system's output, as discussed in Chapter Four. The variance accounted for by the fit to the data ranged from 86%-93%, representing a relatively good fit by the second order model.

Results from the artificial skin sample testing with the DMD are shown in Figures 5.3 and 5.4. The three softer samples, 0.20, 0.21, and 0.22, had mean stiffness values of 221.0 N/m, 292.2 N/m, and 468.6 N/m, respectively, consistent with their rank order. The other three samples had mean stiffness values of 462.4 N/m, 511.8 N/m, and 530.6 N/m, respectively, again consistent with the manufacturer's rank order. The stiffness values for samples 0.22 and 0.23 were not different when evaluated with the DMD.

The 0.20 sample had the highest average damping parameter with a value of 0.83. As the number of the skin sample increased, the damping parameter tended to decrease, with the exception of sample 0.22, which had a lower damping parameter value than sample 0.23. The damping parameter values for the 0.21, 0.22, 0.23, 0.24, and 0.25 samples were 0.82, 0.55, 0.63, 0.60, and 0.53, respectively.

The coefficients of variation for the DMD are given in Table 5.1. They vary across the different sample numbers and between stiffness and damping, but they consistently remain below 5%.

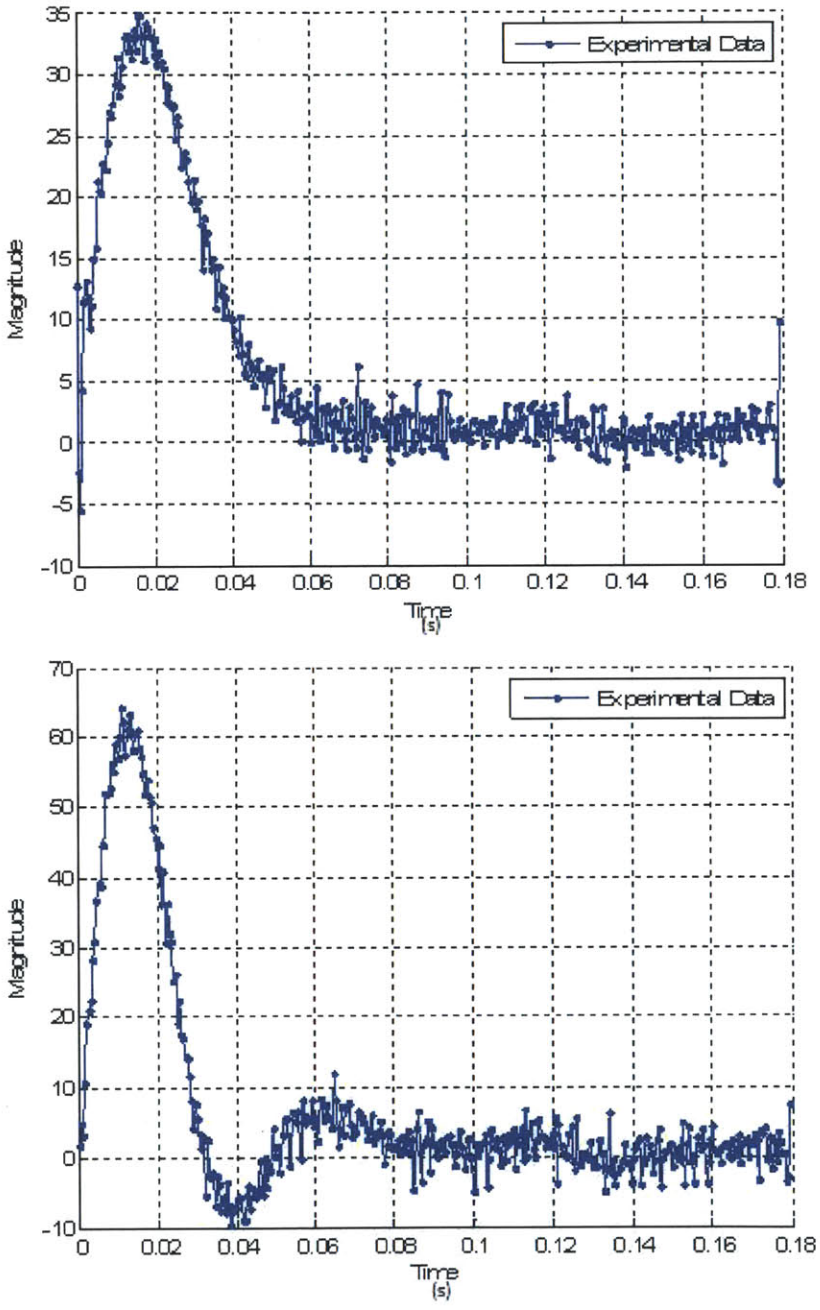

Figure 5.2: Impulse responses for the 0.20 artificial skin sample (top) and the 0.25 artificial skin sample (bottom).

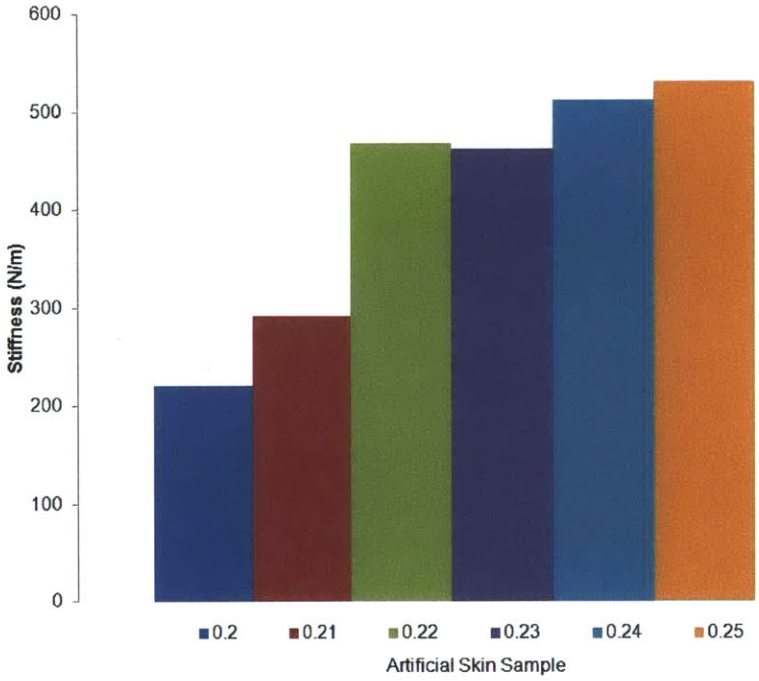

Figure 5.3: Mean stiffness measurements for the artificial skin samples.

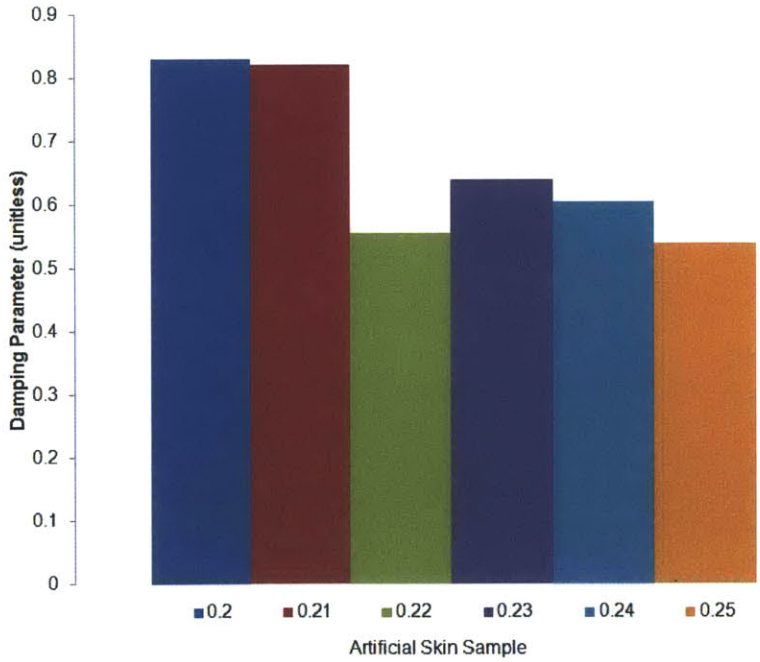

Figure 5.4: Mean damping parameter estimates for the artificial skin samples.

Table 5.2: Results for artificial skin sample testing with the Cutometer.

Artificial Skin Sample Number	R0 (mm)	R5 (unitless)	R6 (unitless)
0.20	0.375	1.085	1.629
0.21	0.227	1.747	2.034
0.22	0.219	1.435	1.550
0.23	0.171	1.903	1.928
0.24	0.103	1.393	1.176
0.25	0.099	1.613	1.349

Table 5.3: Coefficients of variation for Cutometer testing of the artificial skin samples.

Cutometer Parameter	Average Coefficient of Variation
R0	2.6%
R5	5.1%
R6	5.6%

5.1.3.2 Cutometer

The output parameters determined from the data collected using the Cutometer were R0, R5, and R6. These results are shown in Figure 5.5. R0 characterizes the peak of the skin's extension, so the more compliant samples have greater displacements than the stiffer samples. The R5 and R6 parameters do not vary consistently with changes in the samples' stiffness. The results are shown in Table 5.2.

The average coefficients of variation of the Cutometer for this experiment are presented in Table 5.3.

5.1.4 Discussion

The stiffness values measured by the DMD generally increased in the expected direction based on the rank order of samples given by the manufacturer. The exception to this was seen in the stiffness measurements for samples 0.22 and 0.23. The artificial skin samples were only 5 mm thick, so it is likely that the stiffness measurements were influenced by the small thickness of the samples and the hard

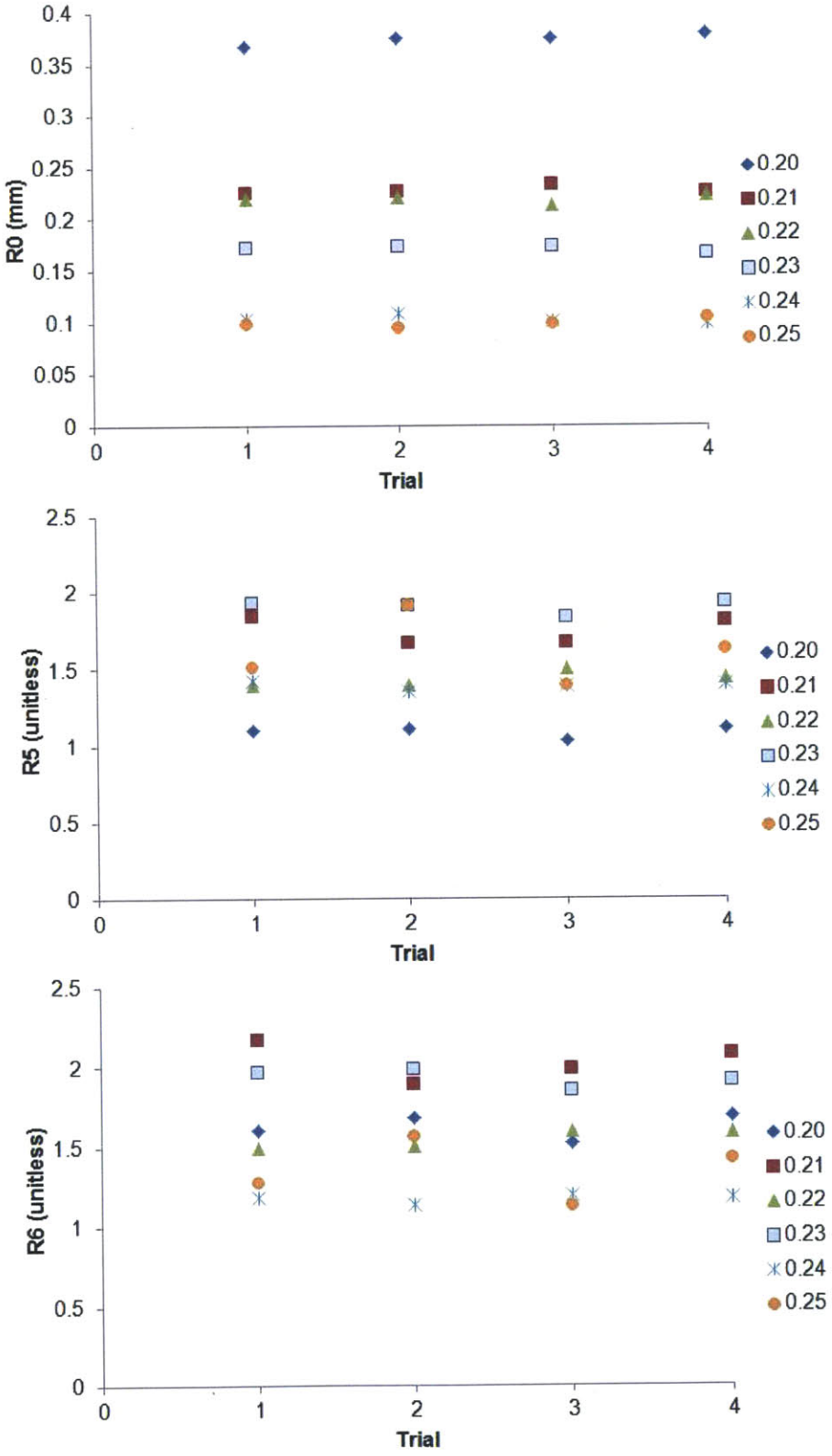

Figure 5.5: R0 (top), R5 (middle), and R6 (bottom) estimates on each trial for artificial skin samples with varying mechanical properties.

surface to which they were affixed. Results of *in vivo* skin testing are affected by the bulk tissue; in this experiment, the hard surface may have contributed to the measurements made on the sample.

The damping parameter values measured in the skin samples reflect the settling time of the system. Systems with lower damping parameters (values between 0 and 1 indicate the system is underdamped), such as those seen in the higher stiffness samples (0.24 and 0.25), oscillate more than those with higher damping parameters, and thus have a longer settling time. The mechanical properties of the higher stiffness samples do not allow perturbations made by the DMD to be damped out as easily as in the lower stiffness samples.

The coefficients of variation for the DMD measurements all remained below 5%, indicating that measurements for each sample were reliable. The coefficients did not vary consistently with the sample's rank order.

The Cutometer's R0 measurements are consistent with the samples' rank order. The stiffest samples displaced the least amount because their mechanical properties did not allow suction from the Cutometer to stretch them. The least stiff samples exhibited the highest displacement because they were more compliant. The R5 and R6 results did not change consistently with the rank order.

The coefficients of variation for the Cutometer are lower than those calculated from testing on human skin, which will be presented later in this chapter. A possible reason for this may be that the skin samples did not move at all during or between measurements. The only parameter with a coefficient of variation of less than 5% was R0, which measures only the linear extension of the skin. The other parameters' coefficients were above 5%, indicating the Cutometer may not be as reliable for these types of measurements.

5.2 Experiment 2: Mechanical Properties of Different Skin Sites

5.2.1 Objective

The goal of this experiment was to determine the reliability and validity of the DMD by measuring the mechanical properties of hairy and glabrous skin and comparing the device's performance with that of the Cutometer. There is a large difference between the thickness of the stratum corneum in glabrous skin compared with hairy skin, and it was hypothesized that the device would be capable of detecting this difference. It was also of interest to see how much the mechanical properties of skin varied across the different sites tested.

Another objective of this experiment was to determine if the DMD was capable of detecting differences in skin stiffness or damping between the male and female subjects tested. Research has shown that males have thicker skin with a higher collagen content than females [29], but several studies in which a variety of devices were used have not been able to detect these differences in mechanical properties [1].

5.2.2 Methods

5.2.2.1 Subjects

Eight subjects were tested. Four were male and four were female, and their ages ranged from 19-55 years. All subjects gave their informed consent to the procedures and all research was approved by MIT's Committee on the Use of Humans as Experimental Subjects.

5.2.2.2 Procedure

Five locations on the forearm and hand were selected for study: the posterior surface of the forearm near the wrist, the anterior surface of the forearm near the wrist, the anterior surface of the forearm near the elbow, the dorsal surface of the

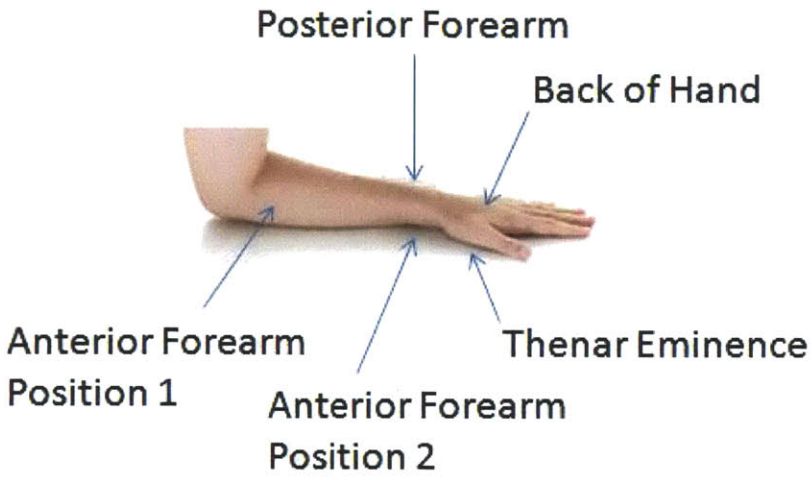

Figure 5.6: Diagram showing the five skin sites tested.

hand, and the thenar eminence, shown in Figure 5.6. The locations near the wrist were approximately 60 mm from the base of the hand. The location near the elbow was 50 mm from the elbow.

The procedure described in Chapter Three was used. Each trial lasted five seconds and eight consecutive measurements were taken at each site.

5.2.3 Results

5.2.3.1 DMD

The inverse Laplace transform of the system's compliance transfer function, given in Equation 4.10, was used to fit the impulse response functions calculated from the measurements made at the skin sites.The variance accounted for by the equation fitted to the skin data ranged from 86% to 94%.

The mean values measured for the stiffness and damping parameters at each of the five sites tested are illustrated in Figures 5.7 and 5.8. The data are shown with the standard error of the mean (SEM). The results are also presented in Table 5.4 along with the percent differences between male and female measurements. A repeated measures analysis of variance (ANOVA) of these data indicated that there

Table 5.4: Group mean results for stiffness and damping from the male and female subject skin sites tested with the DMD. The percent difference between the male and female measurements is also given.

Skin Site	**Mean Female Stiffness (N/m)**	**Mean Male Stiffness (N/m)**	**Percent Difference (Stiffness)**	**Mean Female Damping (unitless)**	**Mean Male Damping (unitless)**	**Percent Difference (Damping)**
Posterior Wrist	259.2	335.4	29.4%	0.5566	0.6449	15.8%
Anterior Wrist	265.6	326.6	23.0%	0.5564	0.6548	17.7%
Anterior Elbow	259.8	303.8	17.0%	0.5515	0.6007	8.9%
Posterior Hand	265.8	308.4	16.0%	0.5414	0.5837	7.8%
Thenar Eminence	393.0	552.6	40.6%	0.6677	0.8214	23.0%

was a significant difference in the stiffness and damping parameters measured at the five sites (stiffness: $F(4,28)=23.09$, $p<0.001$; damping: $F(4,28)=12.27$, $p<0.001$). The highest stiffness and damping parameter values were measured on the glabrous skin on the thenar eminence of the hand.

The mean coefficients of variation for stiffness and damping were calculated for the five sites tested and are presented in Table 5.5. The means for the stiffness and damping estimates were 3.2% and 3.7%, respectively. In general, the coefficients of variation did not vary much as a function of the site tested and ranged from 2.9%-3.6% for stiffness and 3.2%-4.0% for damping.

5.2.3.2 Cutometer

The sites were also tested using the Cutometer. The group mean R0 values are shown in Figure 5.9. The thenar eminence displayed the lowest average R0 value because of its stiffer, thicker epidermis. These properties make the skin site

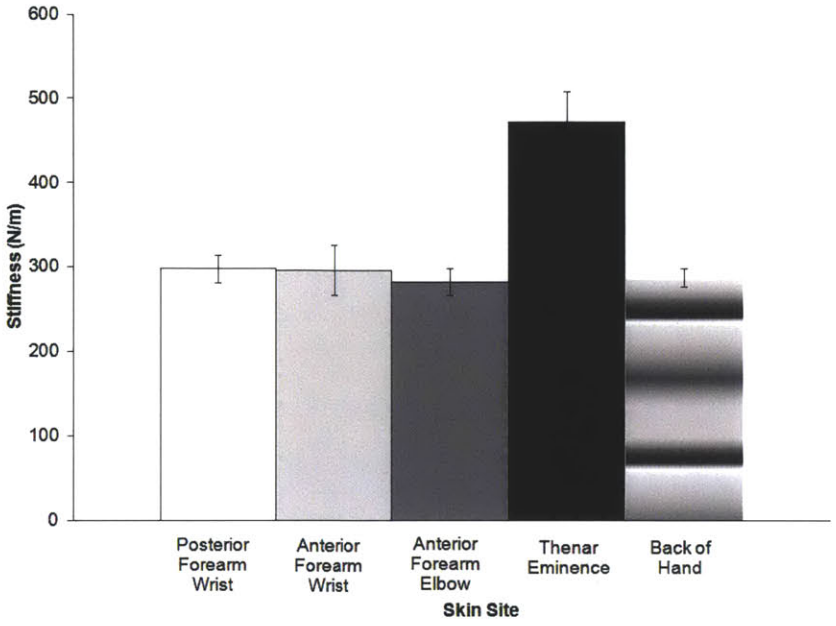

Figure 5.7: Group mean skin stiffness measured at five sites (± SEM).

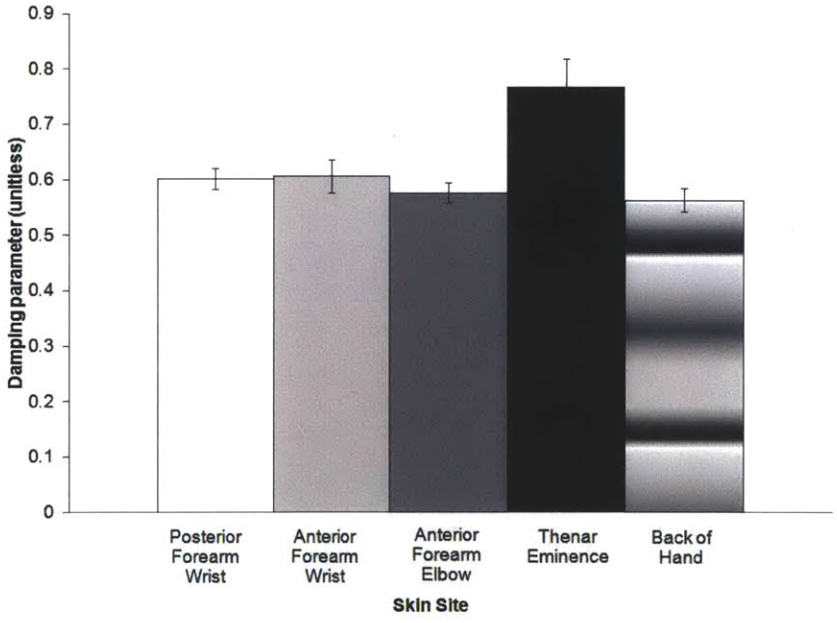

Figure 5.8: Group mean skin damping parameter measurements (± SEM) at five sites.

Table 5.5: Coefficients of variation for skin sites tested with the DMD.

Test Site	Mean CV for Stiffness (male)	Mean CV for Stiffness (female)	Mean CV for Damping (male)	Mean CV for Damping (female)
Posterior Wrist	2.5%	3.3%	4.4%	3.6%
Anterior Wrist	3.2%	4.2%	3.3%	3.9%
Anterior Elbow	3.2%	2.6%	4.6%	2.9%
Thenar Eminence	3.2%	3.5%	2.8%	3.5%
Posterior Hand	3.8%	3.3%	4.4%	4.0%

more resistive to suction than the other sites, resulting in a low R0 value. The anterior elbow, anterior wrist, posterior wrist, back of hand, and thenar eminence had mean R0 values of 0.3611 mm, 0.3331 mm, 0.2225 mm, 0.2757 mm, and 0.1656 mm, respectively. The mean CVs for the three parameters calculated with the Cutometer (R0, R5, and R6) were 5.7%, 6.2%, and 16.6%, respectively.

The relation between the parameters related to the skin's elasticity (R0 and R5) calculated from measurements made with the Cutometer and the stiffness measured by the DMD was evaluated. The correlation coefficients (Pearson product moment) between the R0 and R5 parameters and the stiffness measured by the DMD were -0.53 and -0.51, respectively. These values indicate there was a modest and significant relation ($p<0.01$) between the variables measured with the two instruments. The correlation between the R5 parameter and stiffness was significant at $r=-0.39$ ($p<0.05$).

5.2.4 Discussion

At all five locations tested, higher stiffness and damping parameter values were found in the male subjects; this was particularly evident on the glabrous skin of the thenar eminence of the hand. These findings are assumed to reflect the higher collagen content in the skin of men as compared to women [29]. The stiffness and damping estimates obtained were very similar on the four areas of hairy skin

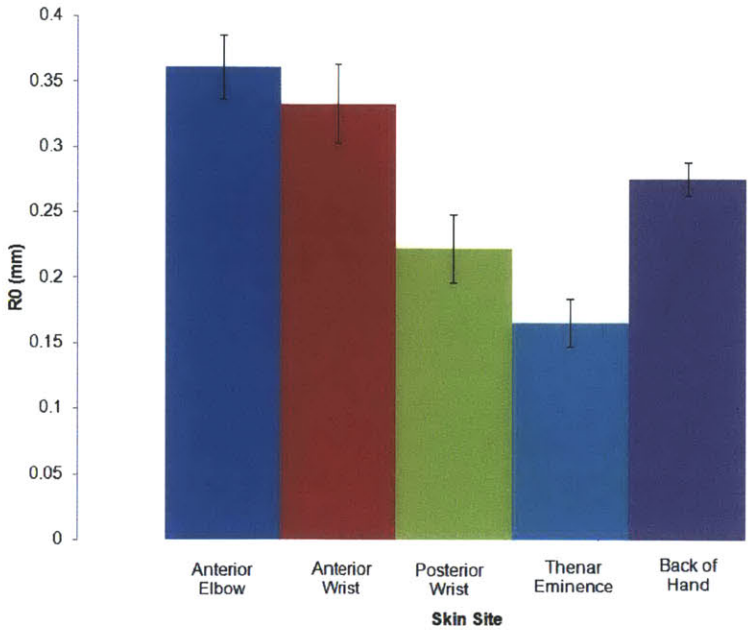

Figure 5.9: Group mean Cutometer R0 results for different skin sites (± SEM).

that were tested and were considerably higher for all subjects on glabrous skin, as expected.

In addition to the difference in the amount of collagen present in the skin, water content may contribute to the higher stiffness values measured in the male subjects. Betz et al. measured skin water content with the Corneometer and found that men had a higher skin water content both before and after the application of formulations [30]. As seen in results from other experiments in the present research, higher water content contributes to higher stiffness. The results from the present experiment indicate that the DMD is a reliable device for distinguishing differences between the skin of men and women.

The coefficients of variation calculated in this experiment were higher than those calculated in Experiment 1. While the artificial skin samples did not move, it is likely that test subjects' arms moved slightly during testing. The arm was constrained so the movements were not large, but the slightest movement may have the potential to alter results between trials.

The correlation between the Cutometer and the DMD indicates there was a modest and significant relation between the variables measured with the two instruments. Differences between the measurements made with the two devices occur for a variety of reasons. The DMD has a high sampling frequency of 2 kHz, whereas the Cutometer samples at a much lower frequency of 100 Hz. The mechanical perturbations caused by the two instruments are also different. The Cutometer relies on the suction method, whereas the DMD moves across the surface of the skin. Finally, the data collected by the devices is analyzed differently. The data from the Cutometer is reported as extension values in mm and ratios of different points along the extension curve, while the DMD reports dynamic values such as stiffness, damping, and natural frequency.

5.3 Experiment 3: Effects of Formulations on Mechanical Properties of Skin

5.3.1 Objective

The objective of the third experiment was to determine how well the device detected changes in the skin's mechanical properties after the application of formulations containing various film forming polymers. The formulations were provided by Procter and Gamble. These polymers act as skin tightening agents and are known to alter the properties of the surface of the skin [11], [31]. They are commonly used in the cosmetic industry to induce skin tightness, which is accompanied by skin smoothing and elimination of wrinkles and lines [31]. It was expected that the formulations containing the highest concentration of the polymers would cause the greatest change in the skin's stiffness.

5.3.2 Methods

5.3.2.1 Subjects

Seven female subjects were tested. Their ages ranged from 19-23 years. All subjects gave their informed consent to the procedures and all research was approved by MIT's Committee on the Use of Humans as Experimental Subjects.

5.3.2.2 Procedure

Four gel formulations were tested, three of which contained high molecular weight water-soluble polymers. These polymers were either polyimide-1, under the name Aquaflex XL-30, or a polyvinylpyrrolidone/acrylate/lauryl methacrylate copolymer under the name of Styleze 2000 (Ashland Specialty Ingredients, Wayne, NJ). The concentrations of tightening agents were 1% Aquaflex, 3% Aquaflex, and 3% Styleze. The fourth formulation contained no film forming polymers and was used as a control to ensure that the carrier gel of the stiffening agents was not contributing to changes in the skin's mechanical properties.

Measurements were first made on untreated, normal skin. All measurements were made on the anterior forearm position 2 shown in Figure 5.6. The formulations were applied to a 3.8 cm diameter circle on the skin with a surface area of 11.34 cm^2 and evenly distributed to form a continuous film, as described in the Jachowicz studies [11], [31]. The films were left on the skin to dry for ten minutes, and then the area was tested again. This drying time was also consistent with the Jachowicz study.

The procedure described in Chapter Three was used. Each trial lasted five seconds and eight consecutive measurements were taken on the forearm.

5.3.3 Results

5.3.3.1 DMD

Compliance impulse response functions for dry skin and each of the four formulations tested are shown for one subject in Figures 5.10 a-e. The data were fitted with Equation 4.10, the inverse Laplace transform of the system. As seen from the fits in the figures (red line) and the VAF which ranged from 88% to 94%, this model provided a good fit to the data.

Figure 5.11 shows the mean stiffness values measured following application of the various formulations and under normal (untreated) conditions. The values for stiffness of the untreated skin ranged from 209 N/m to 230 N/m, consistent with the results obtained in testing different skin sites. Application of the formulated gels to the skin resulted in an increase in its stiffness, with increases ranging from 3.1% to 13.3% (mean 8.6%) for the 1% Aquaflex to 6.2% to 27.4% (mean 13.9%) for the 3% Aquaflex formulation. The 3% Aquaflex and 3% Styleze gels produced average stiffness values of 246 N/m and 244 N/m, respectively. The gel without film forming polymers caused a much smaller change in stiffness that ranged from 0.3% to 1.6%. A repeated measures ANOVA of these data revealed that there was a significant difference in the stiffness of the skin as a function of the formulation applied ($F(4,24)=15.97$, $p<0.001$).

The group mean results illustrated in Figure 5.12 show an overall increase in the damping parameter following application of the gel containing Styleze and both gels containing Aquaflex. However, there was no statistically significant difference in the damping parameter estimates as a function of the formulation applied to the skin ($p=0.35$). The individual subject data were most consistent after application of 3% Styleze, with all subjects showing an increase in the damping parameter. The results were less consistent across subjects following the application of both gels containing Aquaflex. The gel that did not contain film forming polymers caused some change in the damping parameter, although its effect was not clear. The within-subject

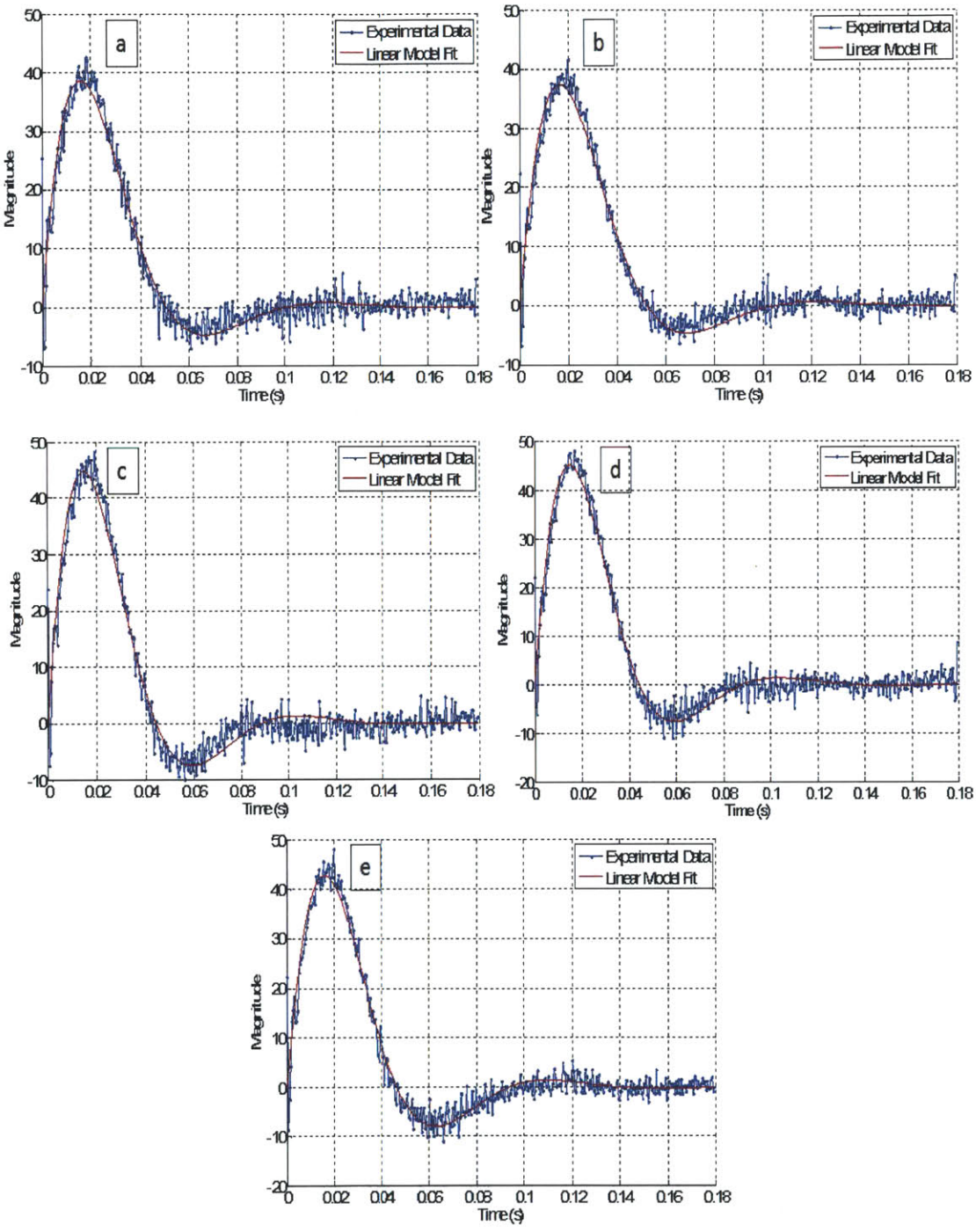

Figure 5.10: Compliance impulse responses from one subject for dry skin (a), without film forming polymers (b), 1% Aquaflex (c), 3% Aquaflex (d), and 3% Styleze (e).

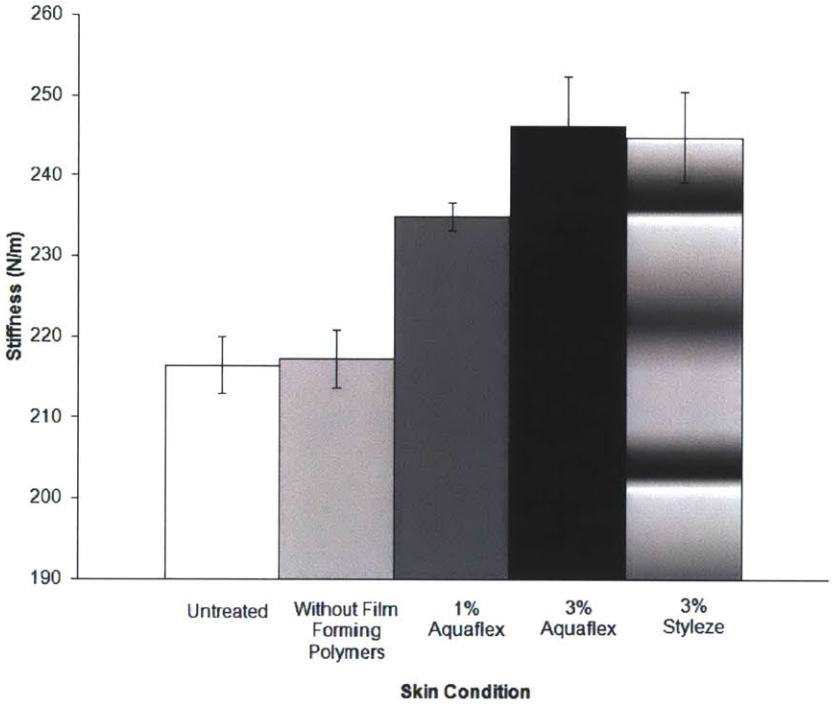

Figure 5.11: Stiffness of skin measured with the DMD on untreated skin and after the application of various film forming polymer gels (± SEM).

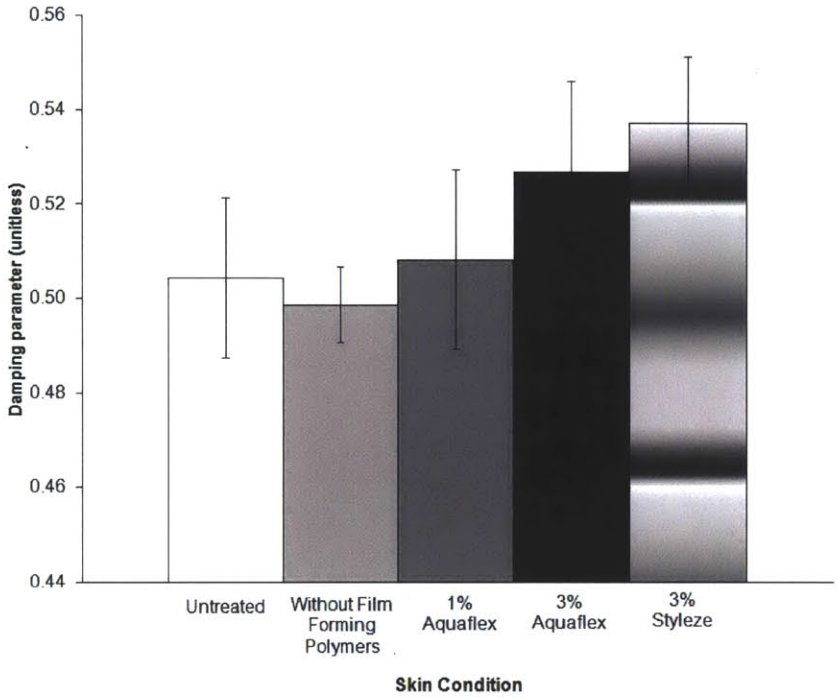

Figure 5.12: Formulation damping results (± SEM).

damping data were nevertheless quite consistent, as reflected in the mean CV of 3.3% across all conditions.

5.3.4 Discussion

The changes in the skin's mechanical properties caused by application of the formulations are visible in the impulse responses illustrated in Figure 5.10. There is essentially no change in the responses denoted a and b, which shows that application of gel without film forming polymers did not result in any significant change in the skin's mechanical properties. These data confirm that any changes measured after the application of the other formulations were caused by the film forming polymers and not the carrier gel. The impulse responses labeled c-e are from skin tested with the 1% Aquaflex, 3% Aquaflex, and 3% Styleze formulations, respectively. The higher peak values indicate the higher stiffnesses observed in skin tested after application of these formulations.

Jachowicz et al. found the Young's modulus (units of N/mm^2) of polymer coated skin to be higher than that of untreated skin, with an average increase ranging from 30.4% ± 9.0% to 115.4% ± 68.0%. The low end of the range corresponds to 1% Aquaflex, while the high end of the range corresponds to 3% Styleze. The 3% Aquaflex formulation induced an average stiffness increase of 54.0% ± 31.3%. This study evaluated the mechanical properties of skin using indentometry [31].

In another study they found a significant increase in skin stiffness after the application of the same film forming polymer gels. This study also used indentometry to evaluate mechanical properties of the skin. Stiffness results were presented in units of N/m, as in the present research. The average stiffness of untreated skin was measured at 37.1 N/m. The 1% Aquaflex gel was found to increase stiffness by a range of 22% to 40%. The ranges for the 3% Aquaflex and 3% Styleze gels were 26% to 53% and 26.1% to 93.4%, respectively [11]. The average stiffness values were lower than those measured in the present research. This is most likely due to the low normal force between the indentometer and the skin; the normal force was kept at 0.06 N for the indentometer, whereas it was maintained between 1.2 and 1.5 N for the DMD.

Consistent with the results from the Jachowicz studies, application of the formulations resulted in a significant increase in skin stiffness in the present experiment. Although the percent increase was not as high as that observed in the previous studies, the standard errors in the present experiments were smaller. Moreover, the stiffness of the skin was determined to increase progressively with higher concentrations of tightening agents. The 3% Aquaflex and 3% Styleze gels produced similar average stiffness values, suggesting that their effects on skin are similar.

Application of the formulations generally resulted in an increase in the damping parameter, but the changes were more variable than those found for stiffness and were not statistically significant. These results indicate that changes in the damping parameter are not as consistent as changes in stiffness caused by film forming polymers. It is possible that other factors in the skin's anatomy contribute to the

damping parameter measurements in a manner that is not yet known.

5.4 Experiment 4: Effect of Changes in Relative Humidity on Skin's Mechanical Properties

5.4.1 Objective

The purpose of this experiment was to determine if the DMD could detect subtle changes of hydration in the skin. It has been shown that at a constant temperature, an increase in the relative humidity of the environment causes an increase in the moisture content of the stratum corneum as demonstrated by a decrease in the skin's electrical impedance [32] or increase in capacitance [27]. This relationship is shown in Figure 5.13.

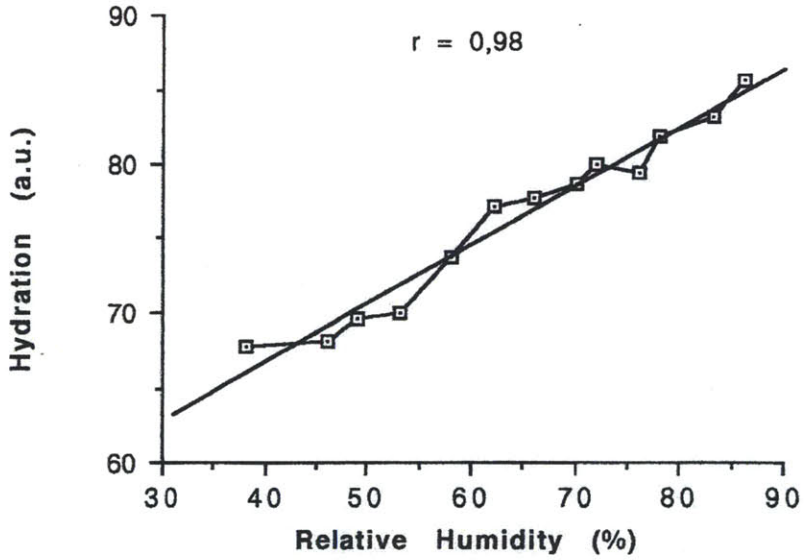

Figure 5.13: Effect of external relative humidity (%) on the capacitance hydration values of the forearm skin. Figure taken from [27].

5.4.2 Methods

5.4.2.1 Subjects

Eight female subjects, ages 19-25, were tested. All subjects gave their informed consent to the procedures and all research was approved by MIT's Committee on the Use of Humans as Experimental Subjects.

5.4.2.2 Procedure

The probe tip was coated with a piece of silicon paper for this experiment because it was suspected that the material of the probe was absorbing some of the moisture on the skin caused by the increased humidity. Because the hydration changes induced by the humidity was more subtle than if the skin had been coated by a product or soaked in water, it was important that it was not absorbed. The normal force between the probe and the skin was also decreased slightly for this experiment and maintained between 1.0 and 1.2 N.

A humidity chamber measuring 30 cm x 30 cm x 40 cm was fabricated from acrylic and connected to an Electro-Tech Systems Model 572 humidifier. To aid the humidifying process, a dish of water was placed in the chamber. To decrease humidity, a section of the chamber was left open to the ambient. The chamber was humidified to three relative humidity levels: 55%, 75%, and 85%. The humidity of the chamber was measured with a Vernier relative humidity sensor and recorded using LabVIEW 10.0 (National Instruments Corp., Auston, TX, USA). The humidity of the chamber was monitored during the entire period the arm was enclosed to ensure conditions remained constant. Relative humidity was maintained within $\pm$ 1.5% of the specified level. The chamber is pictured in Figure 5.14.

After allowing 30 minutes for the subject's skin to adjust to the ambient temperature and relative humidity, a measurement was taken with the DMD and the Cutometer to establish baseline properties of the skin. This follows the protocol established by Clarys that states that subjects should rest at least 30 minutes in the

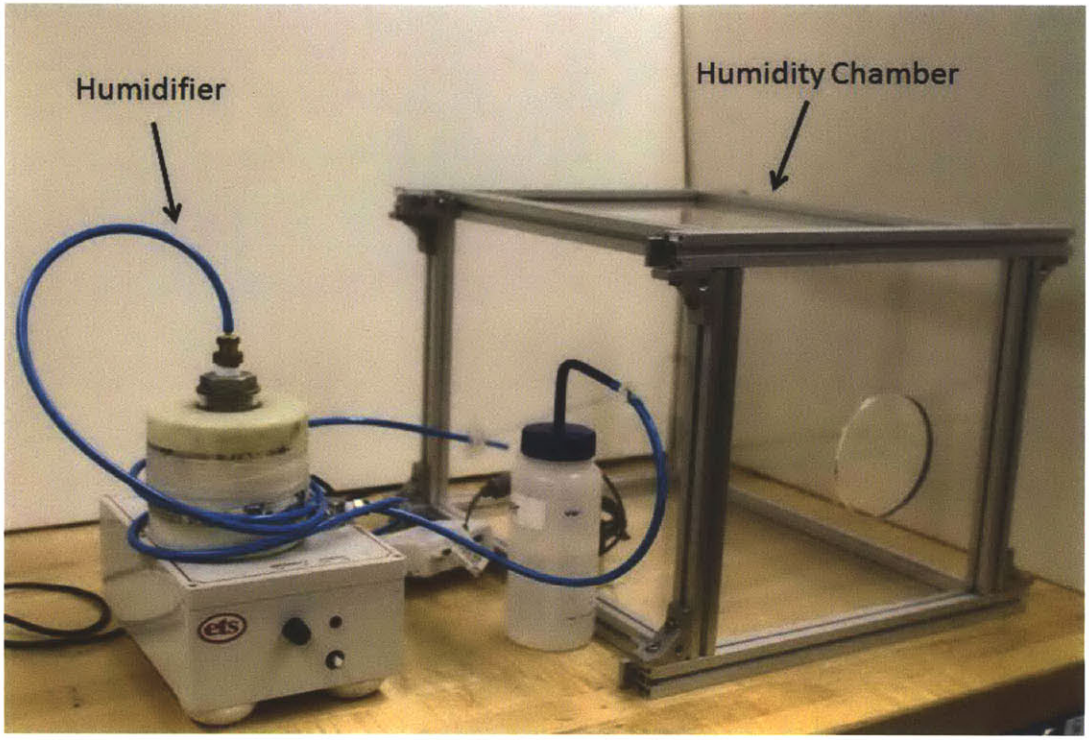

Figure 5.14: The humidity chamber setup.

experimental room before testing to allow their skin to become acclimated to the environment [1]. All measurements for this experiment were taken at the anterior forearm position 2, shown in Figure 5.6. For each relative humidity level, the arm was left in the chamber for 30 minutes. The procedure described in Chapter Three was used. Each trial lasted five seconds and eight consecutive measurements were taken on the arm. Immediately following measurements with the DMD and the Cutometer, the arm was placed back in the chamber for the next level of humidity.

5.4.3 Results

5.4.3.1 DMD

Barel and Clarys [27] have shown that there is a linear relationship between external relative humidity (over the range of 35%-85% RH) and the hydration of the skin as measured by its capacitance. For this experiment, it was assumed that

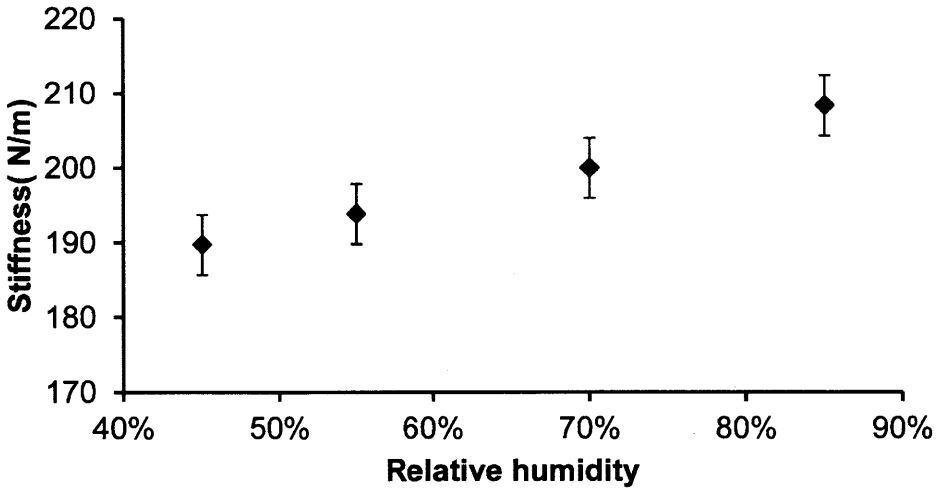

Figure 5.15: Group mean stiffness measurements for the relative humidity levels tested (± SEM). The ambient relative humidity of the room was 45%

after the arm was immersed in the chamber its hydration would increase as predicted by Figure 5.13. The measured relative humidity of the room was 45%. As illustrated in Figure 5.15, the stiffness increased linearly as the relative humidity increased from 45% to 85%. A repeated measures ANOVA of these data indicated that there was a significant increase in stiffness as the hydration of the skin increased ($F(3,21)=9.99$, $p<0.01$). In contrast there was barely any change in the damping parameter measured as the relative humidity increased ($p=0.09$), as shown in Figure 5.16.

5.4.3.2 Cutometer

Results from measurements made with the Cutometer are presented in Figures 5.17, 5.18, and 5.19. The R0 parameter (elastic deformation) increased as the relative humidity increased, consistent with the measurements of stiffness. As evident in Figures 5.18 and 5.19, there was no consistent trend in the R5 and R6 parameter measurements, although the R5 parameter did decrease linearly until the relative humidity reached 70%, and thereafter increased.

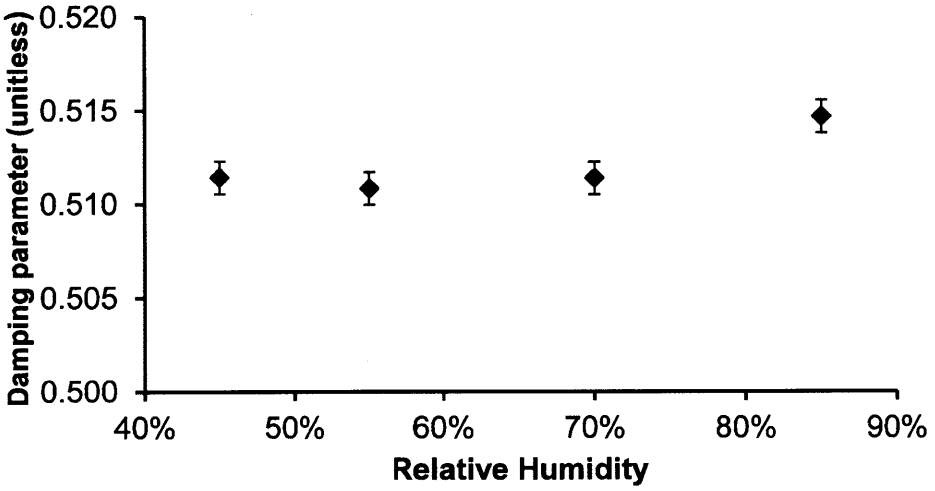

Figure 5.16: Group mean damping parameter measurements for the relative humidity levels tested (± SEM).

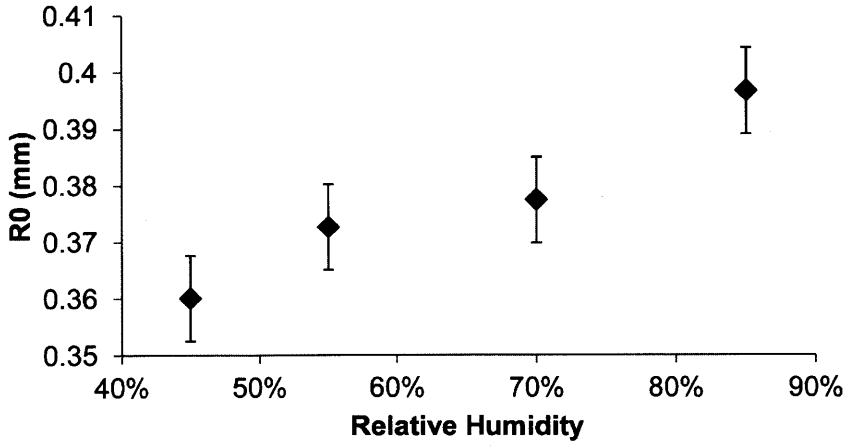

Figure 5.17: Group mean Cutometer R0 results for the relative humidity levels tested.

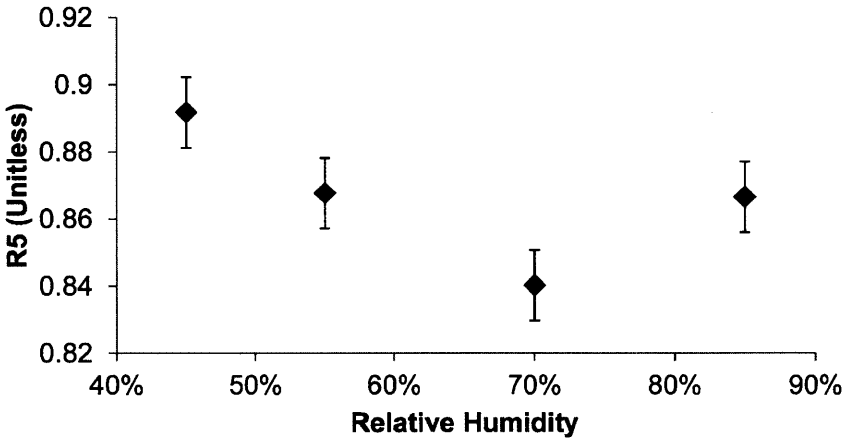

Figure 5.18: Group mean Cutometer R5 results for the relative humidity levels tested.

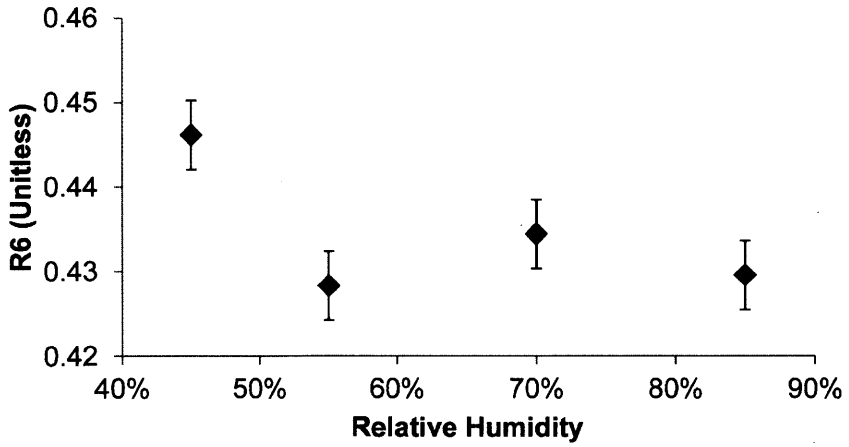

Figure 5.19: Group mean Cutometer R6 results for the relative humidity levels tested.

5.4.4 Discussion

The stiffness of the skin was found to increase linearly as the hydration level of the skin increased, consistent with other experiments that have shown that as the hydration of the skin increases so too does its stiffness [10], [13], and the coefficient of static friction [33], [34], [35]. As the water concentration and distribution in the stratum corneum increases with higher levels of hydration, two separate phenomena occur that contribute to the increase in measured stiffness. One is related to the change in surface tension of the liquid between the skin and the DMD, and the other is hypothesized to involve solubilization of the protein chains in the cells in the stratum corneum [36].

The stiffness measured in this experiment was lower than that measured in the second experiment (Mechanical Properties of Different Skin Sites). This is due in part to the absence of any males in the subject pool for this experiment. The measured stiffness of the male subjects was noted to be on average 25% higher than that of the females in the earlier experiment. Comparing only the female results from Experiment 2 with the present experiment, it can be seen that the average stiffness is still higher in Experiment 2 at the same location with the same ambient conditions (265.6 N/m compared to 189.7 N/m). This is probably due to the smaller normal force used in the present experiment, which was required for the probe to move easily across the hydrated skin surface while absorbing as little moisture from the skin as possible.

These results highlight the importance of conducting *in vivo* skin tests in a controlled environment. Even small changes in relative humidity can have a significant effect on the skin's mechanical properties. The results also suggest that the DMD may be a reliable instrument to use in a clinical setting to measure hydration level in patients. Currently, medical professionals often assess potential dehydration with touch by examining the skin's turgor. The sensitivity of the DMD to changes in relative humidity suggests it could possibly be sensitive enough to detect dehydration. If a standard is established that states that a person is dehydrated if their skin

stiffness measures below a certain amount, the DMD could provide, a fast, efficient way to make clinical measurements.

Chapter 6

Conclusions

This series of experiments revealed that the DMD provides reliable estimates of the mechanical properties of skin. It is capable of differentiating between sites on the body, particularly hairy and glabrous skin, and between the mechanical properties of the skin of women and men. The DMD is sensitive to changes in the hydration of the skin and to the application of thin polymer films. The results from the experiments using the formulations clearly indicate that the DMD can measure the changes in skin stiffness and damping. The effects were consistent across subjects and the device provided reliable data with only a very short period of data collection. The DMD has the additional advantage that it provides estimates of the mechanical properties of skin in physical rather than relative units. This allows direct comparisons between the results from different experiments and from studies using other devices that evaluate the skin's mechanical properties.

The results for the damping parameter were not as consistent as those obtained for stiffness in the experiments. Although there were statistically significant differences in the damping parameters measured at different skin sites, there were no significant changes in the damping parameter in the other experiments. For the subjects tested in Experiment 3, the hydrators containing Aquaflex and Styleze induced an overall increase in the damping parameter, as shown in Figure 5.12. The coefficients of variation remained low for the measurements taken for each subject,

but the average damping parameter across subjects varied greatly. Increasing the number of subjects may provide more definitive results. The damping parameter is not independent of stiffness, although it is dominated by the viscous term B, defined in Equation 4.7. The changes in viscous stiffness generally mirrored the variations in the damping parameter reported for the three experiments.

Compared with the Cutometer, the DMD has more consistent performance. The coefficients of variation for the measurements made with the Cutometer were almost all above 5%, whereas the coefficients associated with measurements made with the DMD all remained below 5%. This could reflect the number of samples taken with each device; the Cutometer was programmed to take four samples at each location, whereas the DMD took eight. The DMD is also able to distinguish between male and female skin unlike the Cutometer, which has not been reported to be able to detect differences in skin associated with a the subject's gender [27].

Compared with the other devices mentioned in Chapter 1, the DMD provides quicker measurements. As previously mentioned, it also provides estimates of the mechanical properties in physical units, unlike the Cutometer, the Corneometer, the Frictiometer, and the Venustron, which all provide estimates in either arbitrary units or unitless ratios. Finally, the DMD outputs both static and dynamic properties of the skin; the devices described in Chapter 1 focus primarily on non-dynamic measurements. None of them measure the damping parameter.

The results from the DMD experiments indicate that the device captures the mechanical responses of the skin as its condition changes, that it produces data that are more consistent than those derived from considerably more expensive commercial devices, and that such measurements can be obtained in a very short period of time. It can be used for both *in vitro* and *in vivo* studies of skin, and has not been shown to affect the mechanical properties of skin so it can be used for repeated measurements. The device has the potential to be useful in clinical and cosmetic settings to make quantitative measurements of the mechanical properties of skin.

The research conducted by Flynn et al. shows that a device capable of measuring

the mechanical properties of skin in multiple axes can give a clearer picture of tissue dynamics [37]. A multi-axis device can measure the skin's anisotropic properties, and provides data from which the skin's nonlinear and viscoelastic characteristics can be evaluated. The next iteration of this device will be designed to operate in three axes. Future work will also focus on augmenting the analytic techniques so that the nonlinear behavior of skin can be characterized, and on developing a portable handheld version of the device.

Bibliography

[1] J. Serup and G. Jemec, Eds., *Handbook of Non-Invasive Methods and the Skin.* CRC Press, Inc., 1995.

[2] G. Boyer, L. Laquieze, A. L. Bot, S. Laquieze, and H. Zahouani, "Dynamic indentation on human skin in vivo: ageing effects," *Skin Research and Technology*, vol. 15, no. 1, pp. 55–67, February 2009.

[3] K. Ashwell, in *Anatomica: The Complete Home Medical Reference*, 2nd ed. Firefly Books Ltd., 2010, pp. 454–479.

[4] L. Slomianka, "Integumentary system," June 2009. [Online]. Available: http://www.lab.anhb.uwa.edu.au/mb140/corepages/integumentary/integum.htm

[5] H. Gray, in *Gray's Anatomy*, 40th ed., S. Standring, Ed. Elsevier Limited, 2008, pp. 523–601.

[6] C. R. Harding, "The stratum corneum: structure and function in health and disease," *Dermatologic Therapy*, vol. 17, pp. 6–15, February 2004.

[7] McGill Molson Medical Informatics Project, "Peripheral sensory mechanisms," 2008. [Online]. Available: http://alexandria.healthlibrary.ca/documents/notes/bom/unit_6/Lec\%2024\%20Peripheral\%20mechanisms.xml

[8] C. Flynn, A. Taberner, and P. Nielsen, "Measurement of the force-displacement response of in vivo human skin under a rich set of deformations," *Medical Engineering and Physics*, vol. 33, pp. 610–619, June 2011.

[9] E. Ruvolo, G. Stamatas, and N. Kollias, "Skin viscoelasticity displays site- and age-dependent angular anisotropy," *Skin Pharmacology and Physiology*, vol. 20, 2007.

[10] H. Dobrev, "Use of cutometer to assess epidermal hydration," *Skin Research and Technology*, vol. 6, pp. 239–244, 2000.

[11] J. Jachowicz, R. McMullen, Y. Zolotarsky, and D. Prettypaul, "Skin tightening with polymer-containing formulations," *Cosmetic Science Technology*, 2005.

[12] J. Jachowicz, R. McMullen, and D. Prettypaul, "Indentometric analysis of in vivo skin and comparison with artificial skin models," *Skin Research and Technology*, vol. 13, no. 3, pp. 299–309, August 2007.

[13] B. Murray and R. Wickett, "Correlations beteen dermal torque meter, cutometer, and dermal phase meter measurements of human skin," *Skin Research and Technology*, vol. 3, no. 2, pp. 101–106, May 1997.

[14] Unpublished, 2012, e-mail correspondence with Courage and Khazaka employee about Cutometer models.

[15] EnviroDerm Services, "Cutometer MPA 580," 2008. [Online]. Available: http://www.enviroderm.co.uk/Cutometer-MPA580

[16] Courage and Khazaka, "CK electronic scientific devices," 2011. [Online]. Available: http://www.courage-khazaka.de

[17] Y. Chen, "Nonlinear stochastic system identification techniques for biological tissues," Master's thesis, Massachusetts Institute of Technology, June 2010.

[18] Y. Chen and I. W. Hunter, "Stochastic system identification of skin properties: Linear and Wiener static nonlinear methods," *Annals of Biomedical Engineering*, 2012, in press.

[19] In-Cosmetics, "Reviscometer." [Online]. Available: http://www.in-cosmetics.com/.../1070/MPA580_Documentation_3.pdf

[20] Dia-stron, "Skin instruments data sheet." [Online]. Available: http://www.diastron.com/images/Skin_Instruments.pdf

[21] DUTECH Scientific, "Courage + khazaka scientific skin test." [Online]. Available: http://www.dutechscientific.com/products_scientific_ck_scientific.php

[22] Axiom, "Venustron." [Online]. Available: http://www.axiom-j.co.jp/venustron.htm

[23] Cortex Technology, "Dermalab skin testing." [Online]. Available: http://www.cortex.dk/dermalab_skin_testing.htm

[24] I. Hunter and M. Korenberg, "The identification of nonlinear biological systems: Wiener and Hammerstein cascade models," *Biological Cybernetics*, vol. 55, pp. 135–144, 1986.

[25] M. J. Korenberg and I. W. Hunter, "Two methods for identifying Wiener cascades having non-invertible static nonlinearities," *Annals of Biomedical Engineering*, vol. 27, pp. 793–804, 1999.

[26] M. J. Korenberg and I. W. Hunter, "The identification of nonlinear biological systems: LNL cascade models," *Biological Cybernetics*, vol. 55, pp. 125–134, 1986, 10.1007/BF00341928. [Online]. Available: http://dx.doi.org/10.1007/BF00341928

[27] A. Barel and P. Clarys, "Measurement of epidermal capacitance," in *Handbook of Non-Invasive Methods and the Skin*, 2nd ed. CRC Press, Inc., 2006, pp. 337–344.

[28] J. Nizet, C. Pierard-Franchimont, and G. Pierard, "Influence of body posture and gravitational forces on shear wave propagation in the skin," *Dermatology*, vol. 202, no. 2, pp. 177–180, 2001.

[29] S. Shuster, M. Black, and E. McVitie, "The influence of age and sex on skin thickness, skin collagen, and density," *British Journal of Dermatology*, vol. 93, pp. 639–643, December 1975.

[30] G. Betz, A. Aeppli, N. Menshutina, and H. Leuenberger, "In vivo comparison of various liposome formulations for cosmetic application," *International Journal of Pharmaceutics*, vol. 296, pp. 44–54, 2005.

[31] J. Jachowicz, R. McMullen, and D. Prettypaul, "Alteration of skin mechanics by thin polymer films," *Skin Research and Technology*, vol. 14, no. 3, pp. 312–319, August 2008.

[32] E. Clar, C. Her, and C. Sturelle, "Skin impedance and moisturization," *Journal of the Society of Cosmetic Chemists*, vol. 26, pp. 337–353, 1975.

[33] S. Comaish and E. Bottoms, "The skin and friction: Deviations from Amonton's laws and the effects of hydration and lubrication," *British Journal of Dermatology*, vol. 84, pp. 37–43, January 1971.

[34] A. El-Shimi, "In vivo skin friction measurements," *Journal of the Society of Cosmetic Chemists*, vol. 28, pp. 37–52, February 1977.

[35] S. Nacht, J. Close, D. Yeung, and E. Gans, "Skin friction coefficient: changes induced by skin hydration and emoillient application and correlation with perceived skin feel," *Journal of the Society of Cosmetic Chemists*, vol. 32, pp. 55–65, 1981.

[36] D. Highley, M. Coomey, M. DenBeste, and L. Wolfram, "Frictional properties of skin," *Journal of Investigative Dermatology*, vol. 69, pp. 303–305, 1977.

[37] C. Flynn, A. Taberner, and P. Nielsen, "Mechanical characterisation of in vivo human skin using a 3d force-sensitive micro-robot and finite element analysis," *Biomechanics and Modeling in Mechanobiology*, vol. 10, pp. 27–38, 2011.

Appendix A

MATLAB

This code was written by Chen for operation of the indentometer [17]. It loads the data collected in LabVIEW into MATLAB and makes linear estimates. It was modified for this research to accommodate multiple runs of the DMD.

A.1 LoadDataAndSequence.m

```
%LoadData

SteppedLinearOutput=zeros(1,21);

exit = false;
count = 1;
filecount = 1;

while(exit==false)

%LoadData;

fileoverwrite = 0;
graphoverwrite = 0;
%Direct File Reading
%file = 'Development/10-07-01/probe3_LAPh_01.lvm';

s1='C:\Documents and Settings\Erika\Desktop\NonlinearSystemID\write files\test';
s2=num2str(filecount);
s3='.lvm';
filename=strcat(s1,s2,s3);
file = filename;


if fileoverwrite == 1;
    file = iteratefile;
end

u = importdata(file, '\t', 24);
[y,indexer]=max(isnan(u.data(:, 6)));
if y ==0, indexer = size(u.data,1); end
timein = u.data(1:indexer-1, 1);
pos = u.data(1:indexer-1, 4);
force = u.data(1:indexer-1, 6);
input = u.data(1:indexer-1, 2);

sampling = timein(2)-timein(1); %Seconds
Fs = 1/sampling; %Hertz

if graphoverwrite ~=1
    %Plot Time Series Data
    figure('Color','w')
    subplot(3,1,1); plot(timein,pos,'r')
    title('Input, Force and Position');
    ylabel('Position (mm)'); grid on
    subplot(3,1,2); plot(timein,force, 'b','MarkerSize',1)
    ylabel('Force (N)'); grid on;
    subplot(3,1,3); plot(timein, input,'k')
    ylabel('Input (V)')
    grid on; xlabel('time')
end
```

```
%Implement filters
startcut = 919*2; %919*2;%2000; %Cut off beginning of signal
graph = 1;
drifttype = 'linear'; %linear, exponential

if graphoverwrite ==1
    graph = iterategraph; %no graphs
end

%Impement drift filter
[posout, param] = driftfilter(pos,input,drifttype, startcut, graph, Fs);

%Implement input frequency filter
band = [10 20];
freqtype = 'none'; %
graph = 0; %no
mymean = 1; %subtract off the mean

postprocess = 1; %truncate series to valid section
[myinput] = myfilter(force(startcut:end), Fs, band, mymean, freqtype, graph, postprocess); %-force
[myoutput] = myfilter(posout(startcut:end), Fs, band, mymean, freqtype, graph, postprocess); %posout

time = timein(end-size(myinput)+1:end);
myvolt = input(end-size(myinput)+1:end);
offsetzero = pos(1000);              %use after 09-04-13

iteration = 0;

graphoverwrite = 0;
if graphoverwrite ~= 1
    figure('Color', 'w')
    subplot(2,1,1)
    autocorr = xcorr(myinput-mean(myinput));
    crosscorr = xcorr(myoutput-mean(myoutput) ,myinput-mean(myinput));
    lagplotter = ((1:1:size(autocorr))-8161)/Fs;
    plot(lagplotter, autocorr/max(autocorr) , 'b'); hold on;
    plot(lagplotter, crosscorr/max(crosscorr), 'r')
    xlabel('Lags (s)')
    ylabel('Scaled Magnitude')
    legend('Input Autocorrelation', 'Input Output Crosscorrelation')
    grid on;

    subplot(2,1,2)
    lagplotter = ((8161:1:8500)-8161)/Fs;
    plot(lagplotter, autocorr(8161:8500)/max(autocorr) , 'b'); hold on;
    plot(lagplotter, crosscorr(8161:8500)/max(crosscorr), 'r')
    xlabel('Lags (s)')
    ylabel('Scaled Magnitude')
    legend('Input Autocorrelation', 'Input Output Crosscorrelation')
    grid on;

    figure('Color','w')
    subplot(1,2,1)
    hist(myinput, 50)
    h = findobj(gca,'Type','patch');
    set(h,'FaceColor','b','EdgeColor','w')
    xlabel('Input Force (N)')
    ylabel('Counts')

    subplot(1,2,2)
    hist((myoutput), 50)
    h = findobj(gca,'Type','patch');
    xlabel('Output Position (mm)')
    ylabel('Counts')
    set(h,'FaceColor','r','EdgeColor','w')

end

downrate = 1;
Fs = Fs/downrate;
myinput = downsample(myinput,downrate);
myoutput = downsample(myoutput,downrate);
time = downsample(time, downrate);
myvolt = downsample(myvolt,downrate);


%SEQUENCE

iteration = 0;
graphoverwrite = 0;
showpower = 1;
showerror = 0;
staticnonlin = 1;
iteron = 1;
plotpriority = 1;  %0=no plots, 1=nonlinear/dynamic plots only, 2=all plots

if graphoverwrite ==1
    plotpriority = iterategraph2; %no graphs
end

if plotpriority>=1
    close all
end
```

```
if iteron ==1 && iteration ==0
    myoriginaloutput = myoutput;    %uses original output first time
    myoriginalinput = myinput;
elseif iteron ~= 1
    myoriginaloutput = myoutput;    %always use provided output
    myoriginalinput = myinput;
end

%Method1 (Toeplitz matrix averaging, works best for shorter impulse responses or changing impulse responses)
noverlap0 = 180; %250; (ms)
nfft = 2*noverlap0;
mywindow = ones(nfft,1); %hanning(nfft); %
[B, SeriesB, StdB, Lags, condition] = myimp(myinput-mean(myinput),myoutput-mean(myoutput), mywindow, noverlap0, nfft, 'condmulti');
%condmulti, grab options from myimp
atry = [0.8; 100; -40];%[0.8; 100; -200]
try
   [Bfit, ahat]=myfit(Lags/Fs, B, atry);
end
%aout = ahat';

%Plot impulse
if plotpriority>0
figure('Color','w','Name', 'Impulse Response'); hold on
plot(Lags/Fs,B*Fs/abs(sum(Bfit)),'.-g'); grid on; hold on %*Fs/abs(sum(B))
plot(Lags/Fs,Bfit*Fs/abs(sum(Bfit)),'k','LineWidth',2); %*Fs/abs(sum(Bfit))
errorbar(Lags(1,1:100)/Fs,B(1,1:100)*Fs/abs(sum(Bfit)),StdB(1,1:100)*Fs/abs(sum(Bfit)), 'LineStyle', 'none', 'Color', 'k');
xlabel('Time'); ylabel('Magnitude'); %title('Impulse Response')
legend('Experimental Data', 'Linear Model Fit')
iRNumb = strcat('ImpulseResponse',num2str(count));
saveas(gcf, iRNumb, 'fig'); %automatically change figure title and save
end

nhat =100;
Bhat = Bhat2(1,1:nhat);
CalcOut = convn(myinput-mean(myinput), B', 'valid')+mean(myinput);
CalcOutHat = convn(myinput-mean(myinput), Bhat', 'valid')+mean(myinput);
FitOut = convn(myinput-mean(myinput),Bfit', 'valid')+mean(myinput);

if plotpriority>1
figure('Color','w', 'Name', 'Time Series Matching')
plot(time(1:size(myoutput,1)), myoutput-mean(myoutput), 'b');
hold on
plot(time(size(B,2):end), CalcOut-mean(CalcOut), 'r');
plot(time(size(Bhat,2):end), CalcOutHat-mean(CalcOutHat), 'm');
plot(time(size(Bfit,2):end), FitOut-mean(FitOut), 'g');
grid on
xlabel('Time (s)'); ylabel('Output');
legend('Actual Measurement', 'Predicted Measurement (Non Parametric)','Predicted Measurement 2 (Non Parametric)', 'Predicted Measurement (Parametric)')
prettyfigure
end

%Measure Error
VAF1 = VAF(myoutput(size(B,2):end)-mean(myoutput(size(B,2):end)), CalcOut-mean(CalcOut));
VAF2 = VAF(myoutput(size(Bhat,2):end)-mean(myoutput(size(Bhat,2):end)), CalcOutHat-mean(CalcOutHat));
VAF3 = VAF(myoutput(size(Bfit,2):end)-mean(myoutput(size(Bfit,2):end)), FitOut-mean(FitOut));

if iteron ==1 && iteration ~=0
    CalcOut0 = convn(myoriginalinput-mean(myoriginalinput), B', 'valid')+mean(myoriginalinput);
    FitOut0 = convn(myoriginalinput-mean(myoriginalinput),Bfit', 'valid')+mean(myoriginalinput);

    VAF10 = VAF(myoriginaloutput(end-length(CalcOut0)+1:end)-mean(myoriginaloutput(end-length(CalcOut0)+1:end)), CalcOut0-mean(CalcOut0));
    VAF30 = VAF(myoriginaloutput(end-length(FitOut0)+1:end)-mean(myoriginaloutput(end-length(FitOut0)+1:end)), FitOut0-mean(FitOut0));

    if plotpriority>1
    figure('Color','w', 'Name', 'Time Series Matching with Original Data')
    plot(time(1:size(myoriginaloutput,1)), myoriginaloutput-mean(myoriginaloutput), 'b');
    hold on
    plot(time(end-length(CalcOut0)+1:end), CalcOut0-mean(CalcOut0), 'r');
    plot(time(end-length(FitOut0)+1:end), FitOut0-mean(FitOut0), 'g');
    grid on
    xlabel('Time (s)'); ylabel('Output');
    legend('Actual Measurement', 'Predicted Measurement (Non Parametric)', 'Predicted Measurement (Parametric)')
    prettyfigure
    end

end

    %Error Stats
    error1 = myoutput(size(B,2):end)-mean(myoutput(size(B,2):end))-(CalcOut-mean(CalcOut));
    error2 = myoutput(size(Bhat,2):end)-mean(myoutput(size(Bhat,2):end))-(CalcOutHat-mean(CalcOutHat));
    error3 = myoutput(size(Bfit,2):end)-mean(myoutput(size(Bfit,2):end))-(FitOut-mean(FitOut));

    if plotpriority>1
    figure('Color','w', 'Name', 'Error Histograms')
    subplot(3,1,1); hist(error1, 100);
    subplot(3,1,2); hist(error2, 100);
    subplot(3,1,3); hist(error3, 100);
    end

    [eacorr1, elags1] = xcorr(error1, myoutput(size(B,2):end));
    [eacorr2, elags2] = xcorr(error2, myoutput(size(Bhat,2):end));
    [eacorr3, elags3] = xcorr(error3, myoutput(size(Bfit,2):end));

    if plotpriority>1
    figure('Color','w','Name', 'Error Cross Correlation')
```

```
    plot(elags1/Fs, eacorr1, 'r'); hold on
    plot(elags2/Fs, eacorr2, 'm');
    plot(elags3/Fs, eacorr3, 'g');
    xlabel('Lags (s)'); ylabel('Cross Correlation'), title('Cross Correlation of Error and Output')
    legend('Error for Prediction 1', 'Error for Prediction 2', 'Error for Prediction (Parametric)')
    end

end

if staticnonlin == 1
    Bused = B; %B or Bfit

    %Estimation of static nonlinearity
    uinput = mean(myinput);
    CalcOut2 = uinput+ 1/Fs*convn(myinput-uinput, Bused'*Fs/abs(sum(Bused)), 'valid');
    if sum(Bused)<0
        Flag = 'Area under impulse response is negative'
    end

    %Static Nonlinearity

        %offset1 = min(CalcOut2);
        %offset2 = min(myoutput(size(Bused, 2):end)); %Define offset2
        offsetzero = min(offsetzero, min(myoriginaloutput)); %min(myoriginaloutput(size(Bused, 2):end)); %

        predicted = @(c,xdat) c(1).*(1-exp(-c(2)*(xdat+c(3))))+offsetzero;
        c0 =[3,0.3,1];

        options = optimset('MaxFunEvals', 1000, 'TolFun', 1*10^(-7), 'LargeScale', 'on');
        [chat, resnorm, residual, exitflag, output, lambda, jacobian]=...
            lsqcurvefit(predicted, c0, CalcOut2, myoriginaloutput(end-length(CalcOut2)+1:end), [], [], options);
        chat;

        outest = chat(1)*(1-exp(-chat(2)*(CalcOut2+chat(3))))+offsetzero;

        if plotpriority>1
        figure('Color','w','Name', 'Time Series Nonlinearity Matching')
        plot(time(end-length(CalcOut2)+1:end), myoriginaloutput(end-length(CalcOut2)+1:end), 'b');
        hold on
        plot(time(end-length(CalcOut2)+1:end), outest, 'r');
        grid on
        xlabel('Time (s)'); ylabel('Output');
        legend('Actual Measurement', 'Predicted Weiner Nonlinearity Model')
        prettyfigure
        end

        VAF4 = VAF(myoriginaloutput(end-length(CalcOut2)+1:end)-mean(myoriginaloutput(end-length(CalcOut2)+1:end)), outest-mean(outest));
        if iteron ==1 && iteration ~=0
            CalcOutOriginal = mean(myoriginalinput)+ 1/Fs*convn(myoriginalinput-mean(myoriginalinput), Bused'*Fs/abs(sum(Bused)), 'valid');
            outestoriginal = chat(1)*(1-exp(-chat(2)*(CalcOutOriginal+chat(3))))+offsetzero;
            VAF40 =  VAF(myoriginaloutput(end-length(outestoriginal)+1:end)-mean(myoriginaloutput(end-length(outestoriginal)+1:end)),
            outestoriginal-mean(outestoriginal));
        end
end


if showpower == 1
    noverlap = 1000;
    nfft = 2*noverlap;
    mywindow =hanning(nfft); %

    %Coherence Plot
    [Cxy,Fc] = mscohere(myinput-mean(myinput), myoutput-mean(myoutput),mywindow,noverlap,nfft,Fs);
     %Power Plot
    [Pxx,Fpx] = pwelch(myvolt-mean(myvolt), mywindow,noverlap,nfft,Fs);
    [Pxx2,Fpx2] = pwelch(myinput-mean(myinput), mywindow,noverlap,nfft,Fs);
    [Pxx3,Fpx3] = pwelch(myoutput-mean(myoutput), mywindow,noverlap,nfft,Fs);

    if plotpriority>1
    figure('Color','w', 'Name', 'Coherence and Input Power'); subplot(2,1,1);
    semilogx(Fc, Cxy, 'LineWidth', 2); grid on
    xlabel('frequency (Hz)'); ylabel('Mean Squared Coherence'); %title('Coherence Squared')

    subplot(2,1,2);
    loglog(Fpx, Pxx, 'LineWidth', 2); hold on;
    loglog(Fpx2, Pxx2,  'r', 'LineWidth', 2);
    loglog(Fpx3, Pxx3, 'k', 'LineWidth', 2); grid on
    legend('Voltage Measured', 'Input', 'Output')
    xlabel('Frequency (Hz)'); ylabel('Power Spectral Density'); %title('Input (From DAQ) Power')
    end
    %Frequency Domain

    [txy, Ft] = tfestimate(myinput-mean(myinput), myoutput-mean(myoutput),mywindow,noverlap,nfft,Fs);
    if plotpriority>0
    figure('Color','w', 'Name', 'TF Estimate')
    subplot(2,1,1);loglog(Ft, abs(txy), 'LineWidth', 2); grid on
    xlabel('Frequency (Hz)'); ylabel('Magnitude'); %title('Estimate of TF')
    subplot(2,1,2);semilogx(Ft, unwrap(angle(txy))*180/pi, 'LineWidth', 2); grid on
    xlabel('Frequency (Hz)'); ylabel('Phase'); ylim([-270 90])
    bPNumb = strcat('BodePlot',num2str(count));
    saveas(gcf, bPNumb, 'fig'); %automatically change figure title and save
    end

end
```

```
iteration = iteration

zeta = sqrt(ahat(3)^2/(ahat(3)^2+ahat(2)^2));
wn = ahat(2)/sqrt(1-zeta^2);
Zeta_wn = [zeta wn]

VAFB = VAF1;
VAFBfit = VAF3;
VAFN = VAF4;
%AICN = AIC4;
Current_VAF = [VAFB VAFBfit VAFN]

if iteron ==1 && iteration ~=0
    VAFB0 = VAF10;
    VAFBfit0 = VAF30;
    VAFN0 = VAF40;
    Original_VAF = [VAFB0 VAFBfit0 VAFN0]
end

Fit_Parameters = ahat'

K = 1000/ahat(1)*wn/sqrt(1-zeta^2)/(Fs/abs(sum(Bfit))); %/Fs
M = K/wn^2;
C = 2*zeta*wn*M;
Linear_Parameters_Scaled = [K M C]

%K2 = 2000/ahat(1)*wn/sqrt(1-zeta^2)/Fs; %/Fs %Change first number according to sampling frequency
K2 = ahat(1)*wn/sqrt(1-zeta^2);
M2 = K2/wn^2;
C2 = 2*zeta*wn*M2;
Linear_Parameters = [K2 M2 C2]

C1 = chat(1);
C2 = chat(2);%/(1000/K)
C3 = chat(3);
Nonlin_Parameters = [C1 C2 C3]


C2actual = chat(2);%/(1000/K2); %using /(1000/K2) will cause divergence even though it is a better representation of the actual system
C3actual = chat(3);%*(1000/K2);

if iteron == 1;
    iteration = iteration+1;
    myoutputest = -1/C2actual*log(1-(myoriginaloutput-offsetzero)/chat(1))-C3actual;
    myoutput = myoutputest;
    time = time(end-length(myoutput)+1:end);
    myinput = myinput(end-length(myoutput)+1:end);
end

%Output
if(count==1)
SteppedLinearOutput = [noverlap0 atry(3) min(pos(startcut:end)) max(pos(startcut:end)) range(pos(startcut:end)) param Current_VAF ...
    Fit_Parameters Zeta_wn Linear_Parameters Linear_Parameters_Scaled sum(Bused)]

else
    beta = [noverlap0 atry(3) min(pos(startcut:end)) max(pos(startcut:end)) range(pos(startcut:end)) param Current_VAF ...
    Fit_Parameters Zeta_wn Linear_Parameters Linear_Parameters_Scaled sum(Bused)];
    SteppedLinearOutput=[SteppedLinearOutput;beta];
end
count = count + 1;
filecount = filecount + 1;

evalResponse = inputdlg('Press 0 to run again, Enter any other number to quit:  ');
fml = strcmp(evalResponse(1),'0');
if(fml)
    exit=false;
else
    exit = true;
end
end

xlswrite('DehydrationDataBeta.xls', SteppedLinearOutput);
```